Chem

CellPress

Article

Structure, Thermodynamics, and Kinetics of Plinabulin Binding to Two Tubulin Isotypes

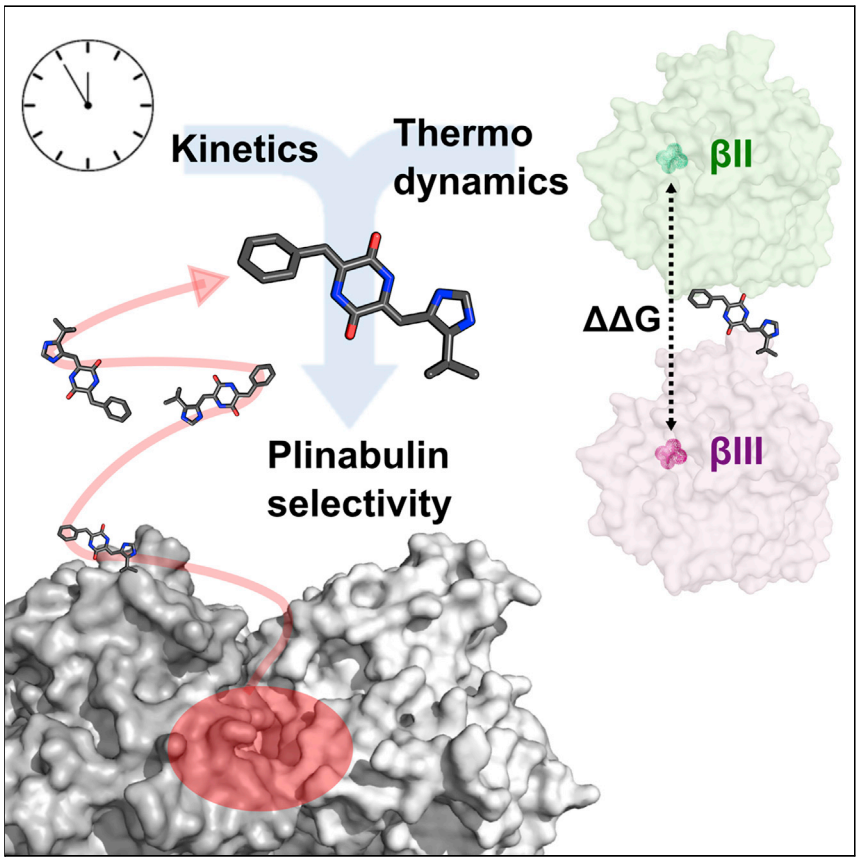

Plinabulin is a novel tubulin-binding agent that is currently in phase 3 clinical trials for cancer treatment and prevention of chemotherapy-induced neutropenia. Plinabulin binds within a distinct tubulin pocket, which differentiates it from other tubulin binders. Aimed at disclosing structural and energetic details of plinabulin binding to tubulin, we combine X-ray crystallography and computational modeling. We compare the plinabulin residence time with that of colchicine and combretastatin-A4. Our study helps understand potential mechanisms underlying differential effects of this family of anti-tubulin drugs.

Giuseppina La Sala, Natacha Olieric, Ashwani Sharma, ..., José Fernando Díaz, Michel O. Steinmetz, Andrea Cavalli

michel.steinmetz@psi.ch (M.O.S.)
andrea.cavalli@iit.it (A.C.)

HIGHLIGHTS

Plinabulin is a phase 3 anticancer and antineutropenia drug candidate

Plinabulin binding to tubulin differentiates it from other compounds

We report crystal structures of plinabulin in complex with βII- and βIII-tubulin isotypes

We performed thermodynamic and kinetic studies on plinabulin selectivity and mechanism of action

La Sala et al., Chem 5, 1–18
November 14, 2019
https://doi.org/10.1016/j.chempr.2019.08.022

Please cite this article in press as: La Sala et al., Structure, Thermodynamics, and Kinetics of Plinabulin Binding to Two Tubulin Isotypes, Chem (2019), https://doi.org/10.1016/j.chempr.2019.08.022

Chem

CellPress

Article

Structure, Thermodynamics, and Kinetics of Plinabulin Binding to Two Tubulin Isotypes

Giuseppina La Sala,[1,2,8,9] Natacha Olieric,[3,9] Ashwani Sharma,[3,9] Federica Viti,[1] Francisco de Asis Balaguer Perez,[4] Lan Huang,[5] James R. Tonra,[5] G. Kenneth Lloyd,[5] Sergio Decherchi,[1,2] José Fernando Díaz,[4] Michel O. Steinmetz,[3,6,*] and Andrea Cavalli[1,7,10,*]

SUMMARY

αβ-Tubulin is a validated target for anticancer drug discovery, and molecules binding to this protein are used to treat several types of tumors. Here, we report on a combined X-ray crystallography and molecular dynamics approach to study drug binding within the colchicine site of αβ-tubulin, focusing on plinabulin, an agent currently in phase 3 clinical testing for the treatment of cancer and chemotherapy-induced neutropenia. We found that plinabulin is more persistently bound to the colchicine site of βII- compared to βIII-tubulin, allowing for a prediction of isotype-expression-dependent drug sensitivity. Additionally, computational residence time and exit paths from the βII-tubulin were compared between plinabulin and two other compounds, colchicine and combretastatin-A4. The former displayed the highest residence time, followed by plinabulin and then distantly by combretastatin-A4. Our combined experimental and computational protocol could help to investigate anti-tubulin drugs, improving our understanding of their mechanism of action, residence time, and tubulin isotype selectivity.

INTRODUCTION

Microtubule-targeting agents (MTAs) are the focus of intense research aiming to improve the treatment of cancer (reviewed in Dumontet and Jordan, 2010[1]). MTAs can be broadly divided into two classes based on their activities toward microtubules at high concentrations: microtubule-stabilizing agents and microtubule-destabilizing agents. In the past few years, structural studies on a plethora of tubulin- and microtubule-MTA complexes have led to the identification and characterization of six different drug binding sites on the αβ-tubulin heterodimer (reviewed in Steinmetz and Prota, 2018[2]). Among them, the colchicine site that is located mostly on the β-tubulin subunit is one of the most versatile sites that interact with a wide variety of very potent ligands belonging to different chemical classes (reviewed in Li et al., 2017[3]). Despite extensive efforts and the discovery of multiple agents, an anticancer drug targeting the colchicine site has not yet reached the market through demonstration of an acceptable risk-benefit profile. A better understanding of the combined structural and kinetic features of binding to the colchicine site for these agents may direct future development in a direction more likely to demonstrate significant efficacy with acceptable tolerability.

It is well known that human cells express different αβ-tubulin isotypes encoded by several α- and β-tubulin genes. One widely recognized resistance mechanism that

The Bigger Picture

Combatting cancer is one of the biggest challenges for improving good health and well-being. Novel anticancer drug candidates have been approved over the last few years, yet many cancers remain as unmet medical needs. Achieving a superior understanding of the molecular mechanism of anticancer drugs is key for designing and developing better compounds in terms of potency and safety profiles. Structural biology and computational studies can help remarkably to investigate the mechanism of action of anticancer drugs. Here, we combine X-ray crystallography with molecular dynamics to investigate structural and energetic properties of drug candidates binding to tubulin, a validated target for the discovery of anticancer medicines. In particular, we study plinabulin, colchicine, and combretastatin-A4, analyzing their mechanism of binding to tubulin, which potentially explains their different functional and safety profiles. We further provide a protocol to study novel tubulin-targeted drugs.

Please cite this article in press as: La Sala et al., Structure, Thermodynamics, and Kinetics of Plinabulin Binding to Two Tubulin Isotypes, Chem (2019), https://doi.org/10.1016/j.chempr.2019.08.022

has emerged for MTAs is the upregulation of specific tubulin isotypes by cancer cells, in particular βIII-tubulin,[4] although in the case of Taxol, this is still a matter of debate.[5] Interestingly, β-tubulin isotypes exhibit significantly different binding affinities toward colchicine, with βIV-tubulin showing the highest binding affinity followed by βII- and βIII-tubulin.[6] In addition, the tubulin-colchicine complex exhibits a slow dissociation reaction and tubulin-isotype-specific binding kinetics.[6–8] A detailed understanding of the differential structural and kinetic properties of colchicine-site binders to different β-tubulin isotypes will, therefore, likely be of value as a first step in selecting cancer types or individual patients for testing. In addition, the crystallographic and molecular dynamics comparison of the binding of different colchicine-site drugs may allow for the determination of binding properties associated with molecules reported to exhibit preferred efficacy and safety profiles in patients to date.

Plinabulin (BPI-2358) is a synthetic analog of the natural product phenylahistin isolated from *Aspergillus* species and is classified as a colchicine-site microtubule-destabilizing agent.[9–12] Several studies have been conducted to shed light on the structure-activity relationships of plinabulin and its derivative.[13–15] The parent plinabulin compound is active against various multi-drug resistant cancer cell lines *in vitro*,[10] and its administration resulted in favorable outcomes in a phase 1 clinical study in patients with advanced malignancies.[16] Moreover, in a phase 2 clinical trial in non-small cell lung cancer (NSCLC) patients with measurable disease, adding plinabulin to docetaxel increased patient overall survival and protected against the development of docetaxel-induced neutropenia. Knowledge of the binding properties of plinabulin to different tubulin isotypes may be useful in developing a strategy to target cancers outside NSCLC. The adverse-effect profile of plinabulin in patients is predominately gastrointestinal and, apart from transient hypertension (on the order of hours), lacks the focus on cardiovascular toxicities (hypertension, tachycardia, bradycardia, QTc prolongation, myocardial infarction, and myocardial ischemia), seen with other colchicine-site-binding agents.[17] Moreover, while plinabulin is utilized to treat chemotherapy-induced neutropenia, other colchicine-site agents such as colchicine and combretastatin-A4 are reported to increase or cause neutropenia.[18,19] Since the adverse-effect profile of plinabulin differs from that of other agents binding to the same pocket of tubulin, detailed colchicine-site structural binding and kinetic comparison among agents may both aid to understand the mechanism of action of plinabulin and inform future molecular drug discovery efforts. Currently, plinabulin is undergoing phase 3 clinical trials for both the treatment of cancer and for the amelioration of chemotherapy-induced neutropenia (CIN).[20,21]

Here, we first solved the crystal structures of plinabulin bound to βII- and βIII-tubulin to 1.5 and 1.8 Å resolution, respectively. We found that residue substitutions in the colchicine site between βII- and βIII-tubulin differentially engage the drug molecule. Using our high-resolution crystal structures, we performed molecular dynamics (MD) and enhanced sampling simulations aimed at gathering detailed information about the thermodynamics and kinetics of plinabulin binding to βII- and βIII-tubulin. Our thermodynamic and kinetic simulation studies suggest a higher affinity of plinabulin toward βII- relative to βIII-tubulin. Importantly, biochemical assays aimed at evaluating the binding selectivity of plinabulin toward the two isotypes confirmed that the compound is more prone to bind to the βII- relative to the βIII-tubulin. We also compared the residence time (i.e., the inverse of k_{off}) of plinabulin within the colchicine site of βII-tubulin with that of colchicine and combretastatin-A4, two drug candidates binding tubulin at the colchicine site.[22,23] Our results suggest that plinabulin shows intermediate unbinding kinetics between the very slow

[1]Computational & Chemical Biology, Istituto Italiano di Tecnologia, via Morego, 30, 16163 Genova, Italy

[2]BiKi Technologies s.r.l., via XX Settembre 33, 16161 Genova, Italy

[3]Laboratory of Biomolecular Research, Department of Biology and Chemistry, Paul Scherrer Institut, 5232 Villigen PSI, Switzerland

[4]Centro de Investigaciones Biológicas, CSIC, 28006 Madrid, Spain

[5]BeyondSpring Pharmaceuticals Inc., 28 Liberty Street, New York, NY 10005, USA

[6]University of Basel, Biozentrum, 4056 Basel, Switzerland

[7]Department of Pharmacy and Biotechnology, Alma Mater Studiorum, University of Bologna, via Belmeloro 6, 40126 Bologna, Italy

[8]Present address: Medicinal Chemistry, Early Cardiovascular, Renal and Metabolism, R&D BioPharmaceuticals, AstraZeneca, 431 83 Mölndal, Sweden

[9]These authors contributed equally

[10]Lead Contact

*Correspondence: michel.steinmetz@psi.ch (M.O.S.), andrea.cavalli@iit.it (A.C.)

https://doi.org/10.1016/j.chempr.2019.08.022

Please cite this article in press as: La Sala et al., Structure, Thermodynamics, and Kinetics of Plinabulin Binding to Two Tubulin Isotypes, Chem (2019), https://doi.org/10.1016/j.chempr.2019.08.022

colchicine off-rate and the very fast unbinding of combretastatin-A4. Together, our study establishes a combined experimental and computational framework to investigate selectivity mechanisms of MTAs against β-tubulin isotypes and residence time of their binding into different tubulin pockets. It further paves the way to design more selective and efficacious anti-tubulin drug candidates for treating cancer and possibly contributes to the explanation of the different pharmacological profiles observed for MTAs.

RESULTS

Crystal Structure of Plinabulin Bound to βII- and βIII-tubulin

The crystal structure of plinabulin bound to bovine brain tubulin (predominantly composed of αI- and βII-tubulin[24]) complexed to darpin D1 (the complex is denoted $T_{\beta II}$D1-plinabulin) was determined at 1.5 Å resolution (Table S1). In agreement with a previous 2.7 Å resolution crystal structure of plinabulin in complex with a macromolecular assembly composed of two tubulin dimers, tubulin tyrosine ligase and the stathmin-like domain of RB3 (T_2R-TTL-plinabulin[12]), the drug binds to the colchicine site of tubulin (Figures 1A and 1B). The colchicine site is formed by helices βH7 and βH8, the βT7 loop, and the βS8 and βS9 strands of β-tubulin and is completed by the αT5 loop of α-tubulin.[25] It can be subdivided into a central pocket (zone 2) and two flanking accessory pockets, one that faces the α-tubulin subunit (zone 1) and the other that is buried deeper in the β-tubulin subunit (zone 3).[26] As shown in Figure 1C, the benzyl and the diketopiperazine-imidazole moieties of plinabulin occupy zones 3 and 2, respectively, which are located mostly on β-tubulin. In contrast, the two archetypical colchicine-site drugs colchicine and combretastatin-A4 occupy zones 1 and 2 in a similar manner and overlap to only a small extent with plinabulin (Figure 1D). Notably, the αT5 loop in the tubulin-plinabulin structure is in a "close" conformation, while the ones seen in the tubulin-colchicine and tubulin-combretastatin-A4 structures adopt a more "open" conformation to accommodate the respective ligands in zone 1 of the colchicine site (Figure 1D).

Several hydrophobic residues of β-tubulin establish van der Waals contacts with plinabulin, including βV238 and βI318 (Figure 1E). Additional hydrogen bonding interactions with plinabulin are established by residues βE200 and βV238 and with residues βG237, βC241, and αT179 via two water molecules (Figure 1E). Notably, the side chain of βC241 is present in two alternate conformations, one of which is forming a hydrogen bond with the carbonyl group of the diketopiperazine moiety of plinabulin (Figure 1E). Interestingly, the βC241 residue is replaced by a serine in the human β-tubulin isotypes βI, βIII, and βVI (Figure S1). We reasoned that the presence of an alternate conformation of the βC241 side chain could be due to a weak interaction of its sulfhydryl group with plinabulin and that the presence of the more polar hydroxyl group of βS241 in βI-, βIII-, or βVI-tubulin isotypes might result in a higher binding affinity toward plinabulin.

To test this hypothesis, we determined the crystal structure of plinabulin in complex with recombinant human αβIII-tubulin[27] bound to darpin D1 (denoted $T_{\beta III}$D1-plinabulin) at 1.8 Å resolution (Table S1). The overall structure of the $T_{\beta III}$D1-plinabulin complex could be readily superimposed with both the $T_{\beta II}$D1-plinabulin complex structure (root-mean-square deviation [RMSD] of 0.258 Å over 896 Cα atoms) and that obtained in the absence of any ligand (PDB ID 4DRX, RMSD of 0.306 Å over 869 Cα atoms). This result suggests that the global conformation of both β-tubulin isotypes is very similar and that plinabulin does not significantly affect their tertiary structures. In agreement with our hypothesis, residue βS241 of the $T_{\beta III}$D1-plinabulin

Please cite this article in press as: La Sala et al., Structure, Thermodynamics, and Kinetics of Plinabulin Binding to Two Tubulin Isotypes, Chem (2019), https://doi.org/10.1016/j.chempr.2019.08.022

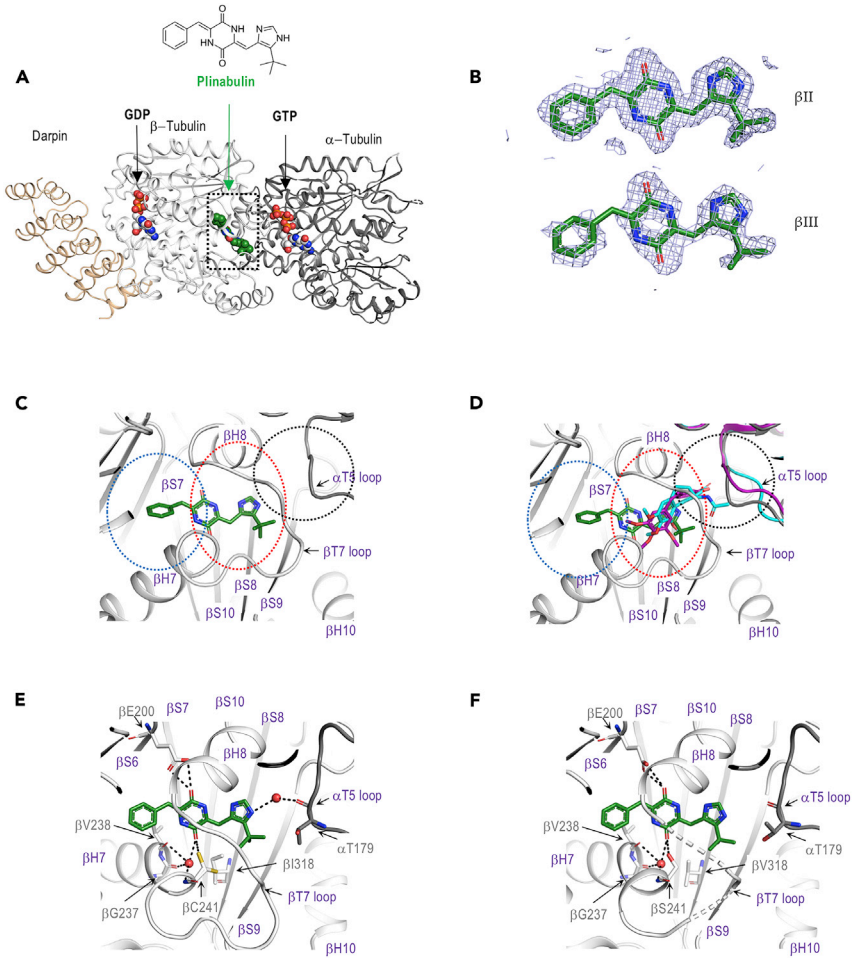

Figure 1. Plinabulin Binds to the Colchicine Site of Tubulin

(A) Overall view of the $T_{\beta II}$D1-plinabulin crystal structure. Plinabulin is displayed as green spheres. The α- and β-tubulin subunits are represented in dark and light gray, respectively. The guanosine nucleotide molecules are shown as spheres and are color-coded according to atom types: carbon, white; oxygen, red; and nitrogen, blue. The dashed black box highlights the region shown in panels (C)–(F).

(B) Fit of plinabulin in the electron density of the $T_{\beta II}$D1-plinabulin and $T_{\beta III}$D1-plinabulin crystal structures. The electron density (blue mesh) is displayed using a sigma-A-weighted 2Fo-Fc map contoured at 1.0 level.

(C) Plinabulin-binding site showing the major secondary structure elements shaping the colchicine site of αβ-tubulin. Three zones in the colchicine site are highlighted by black (zone 1), red (zone 2), and blue circles (zone 3).

(D) Overlays comparing the binding pose of plinabulin to the ones of colchicine (cyan sticks) and combretastatin-A4 (purple sticks).

(E and F) Zoomed-in view of the plinabulin-binding site in the $T_{\beta II}$D1-plinabulin (E) and $T_{\beta III}$D1-plinabulin (F) complex structures. Plinabulin is shown in green sticks representation. Important interacting residues (light gray sticks) are labeled and color-coded according to their atom composition. Water molecules are displayed as red spheres.

structure displayed a single side-chain conformation, and its hydroxyl group was located at an ideal hydrogen-bond distance of 2.8 Å from the carbonyl group of the diketopiperazine ring of plinabulin; in comparison, the sulfhydryl group of βC241 in $T_{\beta II}$D1 is located at a 3.3 Å distance (Figures 1E, 1F, and S5). This observation suggests that plinabulin binds tighter to βIII- than βII-tubulin; however, despite the fact that both complex structures were prepared, processed, and solved exactly

Please cite this article in press as: La Sala et al., Structure, Thermodynamics, and Kinetics of Plinabulin Binding to Two Tubulin Isotypes, Chem (2019), https://doi.org/10.1016/j.chempr.2019.08.022

in the same manner, we noted that the binding site was only partially occupied with plinabulin in the $T_{\beta III}$D1-plinabulin complex. This was substantiated by a less well defined electron density for the ligand (Figure 1B) as well as by the presence of only partial electron density for the βT7 loop that also assumes its alternate conformation observed in the apo form of the colchicine site (data not shown). Along the same line and again in contrast to what we observed in the $T_{\beta II}$D1-plinabulin structure, the water-mediated hydrogen bond between plinabulin and the main chain of αT179 as well as a part of the βT7 loop are absent and poorly resolved, respectively, in the $T_{\beta III}$D1-plinabulin structure (Figure 1F).

The βII- and βIII-tubulin isotypes share an overall sequence identity of 91% (Figure S1). At the colchicine site, only the two plinabulin-interacting residues βC241 and βI318 of βII-tubulin are replaced by a serine and a valine, respectively, in βIII-tubulin. These slight but nevertheless notable amino acid differences prompted us to perform computational studies to investigate the thermodynamic and kinetic profiles of plinabulin binding to the two tubulin isotypes. In particular, we performed MD and enhanced sampling simulations (i.e., thermodynamic integration [TI] and scaled MD) using both the structures of plinabulin bound to βII- and βIII-tubulin as starting points.

Free Energy of Plinabulin Binding to βII- and βIII-Tubulin

Initially, we employed the molecular mechanics Generalized Born surface area (MM/GBSA) approach,[28,29] a fast and efficient method that is widely utilized for estimating binding affinities (ΔG_{bind}) using MD-derived conformational ensembles. To this end, we performed ~100 ns of classical MD simulations for both the βII-tubulin-plinabulin and βIII-tubulin-plinabulin systems, and then we computed the ΔG_{bind} via the MM/GBSA formalism (see Experimental Procedures for details). The estimated ΔG_{bind} was very similar between the two tubulin isotypes, being -36.28 ± 2.95 kcal/mol for βII-tubulin-plinabulin and -36.06 ± 3.47 kcal/mol for βIII-tubulin-plinabulin. However, since the entropic contribution is neglected in these calculations, these values mainly account for the enthalpic components of the binding free energies.

To better describe the binding process and get a more accurate estimation of the binding energy, we carried out more rigorous physics-based free energy calculations via TI. For this, we computed the binding free energy difference ($\Delta\Delta G_{bind}$) between the βII-tubulin-plinabulin and βIII-tubulin-plinabulin systems (forward and backward to ensure convergence) by performing multi-step alchemical transformations, which gradually mutated the colchicine site from βII- to βIII-tubulin and vice versa. Then, using the TI formalism (Figure 2), we calculated the free energy loss or gain over these transformations. We first computed the $\Delta\Delta G_{bind}$ associated to the βII → βIII transformation, mutating βC241 to serine and subsequently βI318 to valine (Figure 2B). We found that the βC241 → βS241 transformation (denoted βII/TR_1; Table 1) has an energetic cost of $\Delta\Delta G_{bind[\beta II/TR1]} = 0.88$ kcal/mol, being in favor of βII-tubulin. Similarly, also the βI318 → βV318 transformation (denoted βII/TR_2; Table 1) is slightly in favor of βII-tubulin showing a $\Delta\Delta G_{bind[\beta II/TR2]}$ of 0.29 kcal/mol. Together, the two transformations showed an overall $\Delta\Delta G_{bind[\beta II \rightarrow \beta III\text{-}like]} = 1.07$ kcal/mol, with a more favorable binding free energy for plinabulin in complex with βII-tubulin relative to βIII-tubulin.

To check the convergence of both transformations (βII/TR_1 and βII/TR_2; Table 1), we also performed the backward TI starting from the mutated βII-tubulin (βC241S and βI318V) and alchemically transforming it back into the wild-type βII-tubulin (Figure 2B). To this end, we mutated βV318 to isoleucine (denoted βII/TR_3; Table 1), obtaining a $\Delta\Delta G_{bind[\beta II/TR3]}$ of −0.46 kcal/mol. Then, we used the same

Please cite this article in press as: La Sala et al., Structure, Thermodynamics, and Kinetics of Plinabulin Binding to Two Tubulin Isotypes, Chem (2019), https://doi.org/10.1016/j.chempr.2019.08.022

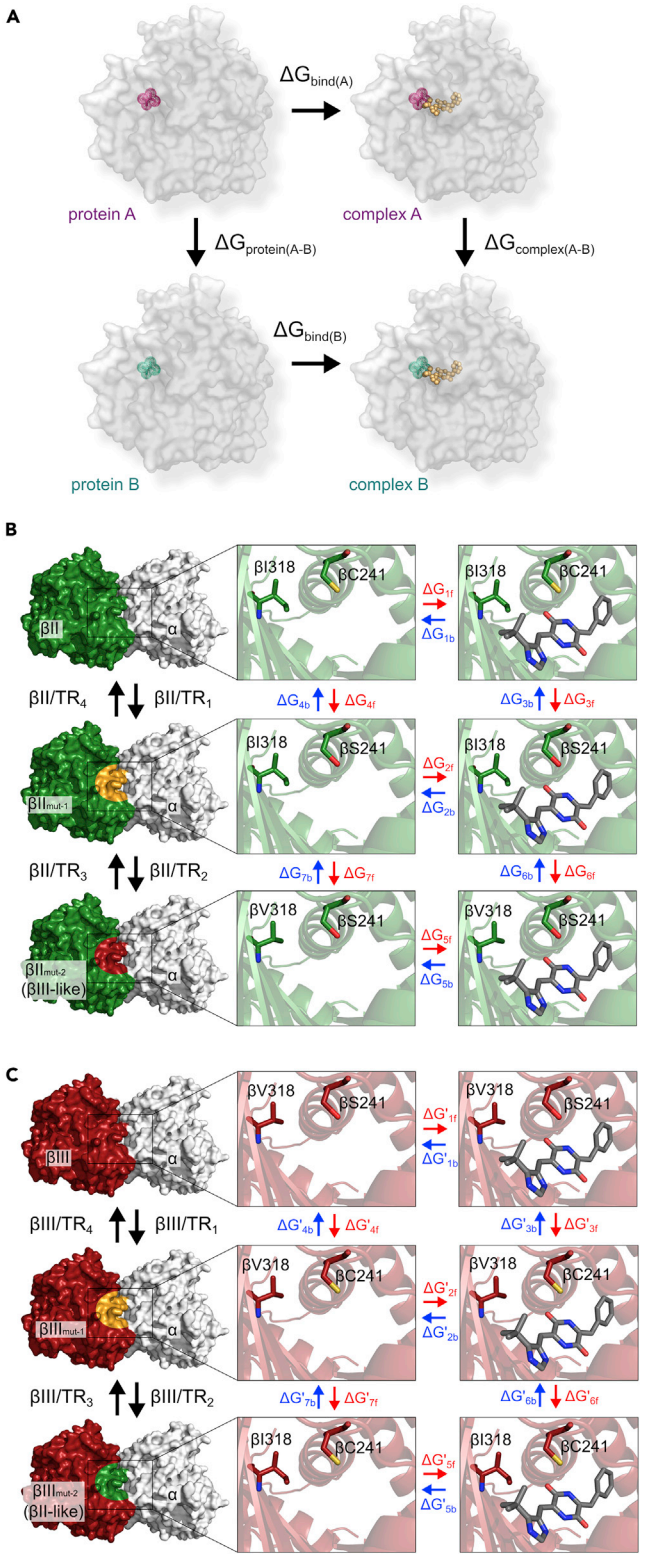

Figure 2. Scheme of the Thermodynamic Cycle

(A) General scheme of the thermodynamic cycle used to calculate the relative binding free energy difference between the ligand in complex with protein A (upper-right) and the ligand in complex

Please cite this article in press as: La Sala et al., Structure, Thermodynamics, and Kinetics of Plinabulin Binding to Two Tubulin Isotypes, Chem (2019), https://doi.org/10.1016/j.chempr.2019.08.022

Figure 2. *Continued*

with protein B (lower-right). In this example, protein A and B can either be the wild type or the mutated tubulin form since both the forward and the backward transformations have been performed. The horizontal legs correspond to the binding process in system A (upper, $\Delta G_{bind(A)}$) and in system B (lower, $\Delta G_{bind(B)}$). The vertical legs correspond to the alchemical transformations of protein A into protein B in the apo form (left, $\Delta G_{protein(A-B)}$) and in complex with the ligand (right, $\Delta G_{complex(A-B)}$). The TI is used to estimate the free energy associated with the vertical legs of the cycle. The relative binding free energy difference ($\Delta\Delta G_{bind}$) is the difference between $\Delta G_{complex(A-B)}$ and $\Delta G_{protein(A-B)}$.

(B) Representation of the alchemical transformations performed in this work. Starting from the βII-tubulin system, we first mutated βC241 to serine (βII/TR_1) to obtain the βII_{mut-1} system and then βI318 to valine (βII/TR_2) to obtain a new βII-tubulin system having a βIII-like colchicine site (βII_{mut-2}). The binging free energy associated to the βII/TR_1 and βII/TR_2 transformations are given by the formulas $\Delta\Delta G_{bind[\beta II \rightarrow \beta II\ mut-1]} = \Delta G_{3f} - \Delta G_{4f}$ and $\Delta\Delta G_{bind[\beta II\ mut-1 \rightarrow \beta II\ mut-2]} = \Delta G_{6f} - \Delta G_{7f}$, respectively (where "f" stands for "forward"). Therefore, the total binding free energy to transform the wild-type βII to βII having a βIII-like colchicine site (i.e., $\Delta\Delta G_{bind[\beta II \rightarrow \beta III\text{-}like]}$) is the sum of $\Delta\Delta G_{bind[\beta II \rightarrow \beta II\ mut-1]}$ and $\Delta\Delta G_{bind[\beta II\ mut-1 \rightarrow \beta II\ mut-2]}$. Starting from the βIII-tubulin like system, we also performed the backward transformations (βII/TR_3 and βII/TR_4) to obtain again the wild-type βII-tubulin system.

(C) Starting from the βIII-tubulin system, we first mutated βS241 into cysteine (βIII/TR_1) to obtain βIII_{mut-1} and then βV318 to isoleucine (βIII/TR_2) to obtain a new βIII-tubulin system having a βII-tubulin-like colchicine site (βIII_{mut-2}). The binging free energy associated to the βIII/TR_1 and βIII/TR_2 transformations are given by the formulas $\Delta\Delta G_{bind[\beta III \rightarrow \beta III;\ mut-1]} = \Delta G'_{3f} - \Delta G'_{4f}$ and $\Delta\Delta G_{bind[\beta III\ mut-1 \rightarrow \beta III\ mut-2]} = \Delta G'_{6f} - \Delta G'_{7f}$, respectively. The total binding free energy to transform the wild-type βIII-tubulin to βIII-tubulin mut-2 (i.e., $\Delta\Delta G_{bind[\beta III \rightarrow \beta III\ mut-2]}$) is the sum of $\Delta\Delta G_{bind[\beta III \rightarrow \beta III\ mut-1]}$ and $\Delta\Delta G_{bind[\beta III\ mut-1 \rightarrow \beta III\ mut-2]}$. Also, here we performed the backward transformation (βIII/TR_3 and βIII/TR_4) to obtain again the wild-type βIII-tubulin system.

approach to transform βS241 into cysteine (denoted βII/TR_4; Table 1), obtaining a $\Delta\Delta G_{bind[\beta II/TR4]}$ of −1.27 kcal/mol. The two transformations showed an overall $\Delta\Delta G_{bind[\beta III\text{-}like \rightarrow \beta II]}$ of −1.73 kcal/mol, which is in very good agreement with the forward transformation (1.07 kcal/mol), suggesting that plinabulin binding is thermodynamically favored in the βII-tubulin isotype.

In light of the small free energy difference, we improved the reliability of our results by performing TI with the structure of plinabulin bound to βIII-tubulin as a starting point and transforming the two key residues of the colchicine site into those of the βII-tubulin isotype (βS241C and βV318I, Figure 2C). As a result, we found that both the βS241 → βC241 and βV318 → βI318 (denoted as βIII/TR_1 and βIII/TR_2, respectively; Table 1) are favored, showing a $\Delta\Delta G_{bind}$ of −1.63 and −0.58 kcal/mol, respectively (the overall $\Delta\Delta G_{bind[\beta III \rightarrow \beta II\text{-}like]}$ is −2.21 kcal/mol). Here too, we carried out the backward transformation to assess the convergence of our simulations. We started from the mutated βIII-tubulin system (βC241S and βI318V) and transformed it into wild-type βIII-tubulin (Figure 2C). Similarly to the protocol reported above, we first mutated βI318 to valine (denoted as βIII/TR_3; Table 1) and then βC241 to serine (denoted βIII/TR_4; Table 1) and obtained a $\Delta\Delta G_{bind}$ of 1.06 and 1.45 kcal/mol, respectively (the overall $\Delta\Delta G_{bind[\beta III\text{-}like \rightarrow \beta III]}$ is 2.51 kcal/mol). These results show that the forward and backward alchemical transformations have strikingly similar absolute values (2.21 versus 2.51 kcal/mol). These calculations further showcase that plinabulin binding is thermodynamically favored for the βII-tubulin isotype relative to βIII-tubulin.

Plinabulin Selectivity Investigated through Biochemical Assays

To obtain evidence for the predicted differential interaction of plinabulin with βII- and βIII-tubulin, we assessed the biochemical activity of the drug on bovine brain tubulin that is composed of 58% βII, 25% βIII and 17% other tubulin isotypes.[30] To this end, we analyzed the composition of βII- and βIII-tubulin present in unassembled

Please cite this article in press as: La Sala et al., Structure, Thermodynamics, and Kinetics of Plinabulin Binding to Two Tubulin Isotypes, Chem (2019), https://doi.org/10.1016/j.chempr.2019.08.022

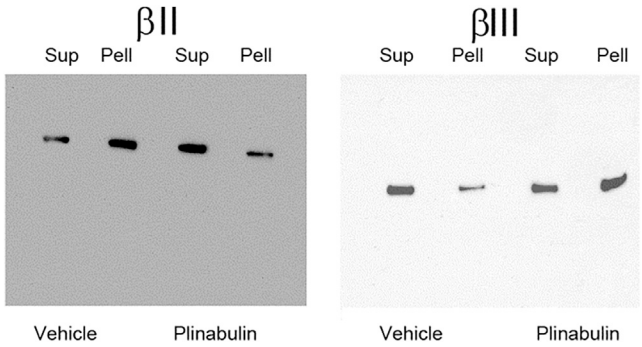

Figure 3. Plinabulin Selectivity Investigated through Biochemical Assays

Differential effect of plinabulin in the assembly of βII- and βIII-tubulin isotypes of calf brain tubulin (60 μM). Representative western blots (the experiment was repeated thrice) of the tubulin isotype contents of supernatants and pellets of 60 μM tubulin assembled in the absence and presence of 5 μM plinabulin. Sup, supernatant; Pell, pellet.

and assembled bovine brain tubulin (60 μM), which was incubated in the absence and presence of 5 μM plinabulin using a standard microtubule pelleting assay[31] in combination with western blotting against both isotypes. The idea behind this experiment is that the tubulin isotype that interacts better with the drug will be prevented to a greater extent from assembly into microtubules compared to the absence of any drug.

Consistent with previous findings[32] in absence of plinabulin, βII-tubulin is more prone to assemble into microtubules as compared to βIII-tubulin, as is shown by the ratios between tubulin isotypes in the supernatant and in the pellet in the presence and absence of tubulin, respectively (Figure 3). These results indicate that in a competitive environment in which both βII- and βIII-tubulin isoforms are available for incorporation into microtubules, plinabulin will increase the relative probability for βIII-tubulin incorporation over βII-tubulin, supporting our structural and computational results that plinabulin preferentially interacts with βII- compared to βIII-tubulin.

Residence Time of Plinabulin and Comparison to Colchicine and Combretastatin-A4

We next focused on the unbinding kinetics by investigating the residence time of plinabulin in the two tubulin isotypes. We utilized scaled MD (SMD) simulations, an enhanced sampling method that enables sampling of rare events, including ligand unbinding, as recently reported for different pharmaceutically relevant case studies.[33–37] We ran multiple replicas (20 for each system) of SMD simulations of both βII- and βIII-tubulin-plinabulin systems. Unlike the free energy calculations reported above, we here modeled the two glutamate-rich and disordered C-terminal tails of both α- and β-tubulin to take into account the possible role these highly negatively charged flexible moieties could play upon ligand unbinding (see the Supplemental Information). We found that the mean scaled residence time of plinabulin in the βII-tubulin isotype was 71.0 ± 10.0 ns, whereas in the βIII-tubulin, it was 52.7 ± 8.2 ns. Therefore, the release of bound plinabulin is slightly slower from the βII- than from βIII-tubulin system, in agreement with the thermodynamics calculations reported above.

We next analyzed the exit paths of the ligand from the colchicine site. This analysis was performed by monitoring the center of mass (COM) of plinabulin along the unbinding trajectories. We found three possible exit routes, denoted as path A, B,

Please cite this article in press as: La Sala et al., Structure, Thermodynamics, and Kinetics of Plinabulin Binding to Two Tubulin Isotypes, Chem (2019), https://doi.org/10.1016/j.chempr.2019.08.022

Table 1. List of Transformations Performed for TI Studies, along with the ΔG Values of Each Transformation

Transformation	Simulation's Name	Starting System	Final System		ΔG (kcal/Mol)
βII to βIII	βII/TR_1	βC241 βI318	βS241 βI318	*forward*	0.88
	βII/TR_2	βS241 βI318	βS241 βV318		0.29
	βII/TR_3	βS241 βV318	βS241 βI318	*backward*	−0.46
	βII/TR_4	βS241 βI318	βC241 βI318		−1.27
βIII to βII	βIII/TR_1	βS241 βV318	βC241 βV318	*forward*	−1.63
	βIII/TR_2	βC241 βV318	βC241 βI318		−0.58
	βIII/TR_3	βC241 βI318	βC241 βV318	*backward*	1.06
	βIII/TR_4	βC241 βV318	βS241 βV318		1.45

and C in Figures 4A and S6. In the vast majority of the trajectories, plinabulin unbound tubulin through path A that involves leaving the colchicine site through a small channel located between the α- and β-tubulin subunits and delimited by the three loops βH7-βH8, βS8-βH10, and αH6-αH7 (colored in orange in Figures 4A and S6). Notably, we also found that in path A, the ligand could stop over in a transient pocket at the αβ-tubulin intradimer interface before leaving the protein. Interestingly, this observation is in line with experimental data reported by Yamazaki et al.,[38] who have suggested that plinabulin could indeed also bind to this region of tubulin. In one simulation for the βII- and in two for the βIII-tubulin systems, ligand unbinding occurred through path B. In this path, the ligand went across a small channel at the αβ-tubulin intradimer interface, in the proximity of loop βH1-βS2 and helix αH2 (colored in red in Figures 4A and S6). Finally, in four SMD simulations of both systems, plinabulin unbound tubulin through path C. Here too, the ligand went across the αβ-tubulin intradimer interface in the proximity of helices βH10 and αH6 (colored in green in Figures 4A and S6).

Interestingly, SMD trajectories also showed that plinabulin could adopt two possible poses within the colchicine site of βII-tubulin. In particular, above the 75th percentile among the collected data, plinabulin was found in two main clusters, referred to as *c1* and *c2* (see red dots in Figures 4B and S2). The *c1* cluster corresponds to the crystallographic binding pose, while the *c2* cluster corresponds to a slightly shifted pose where the phenyl ring of plinabulin finds space in an adjacent deep pocket in the colchicine site (see Figures 4B and S2). Notably, the crystal structure of βII-tubulin in complex with a plinabulin derivative containing an acetophenone group revealed that this moiety indeed exploits this additional pocket.[39] Conversely, the same analysis performed on the MD trajectories collected with the βIII-tubulin system revealed that the most probable binding pose of plinabulin (i.e., above 75th percentile) is the crystallographic one, which is recapitulated by cluster *c1*. These results show that the relative population of poses of plinabulin may vary between the two tubulin isotypes most likely as a consequence of a different plasticity of their respective colchicine sites.

To compare the unbinding kinetics of plinabulin with other colchicine-site ligands, we studied colchicine and combretastatin-A4. To this end, we employed the same

Please cite this article in press as: La Sala et al., Structure, Thermodynamics, and Kinetics of Plinabulin Binding to Two Tubulin Isotypes, Chem (2019), https://doi.org/10.1016/j.chempr.2019.08.022

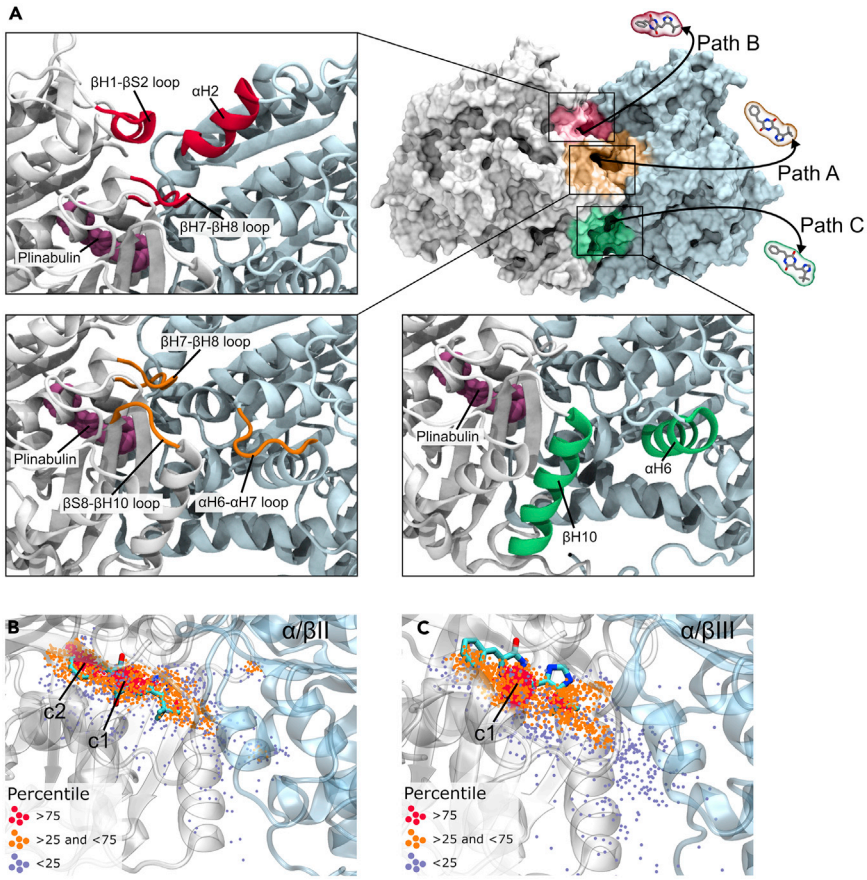

Figure 4. Unbinding Paths of Plinabulin

(A) Unbinding paths observed during our SMD simulations of both βII-tubulin-tail-plinabulin and βIII-tubulin-tail-plinabulin systems. The three "exit channels" are highlighted in orange, red, and green for paths A, B, and C, respectively. The white surface represents the β subunit, whereas the cyan surface indicates the α subunit. The "H" stands for helix, whereas the "S" stands for β-strand. (B and C) Representation of the probability to find the COM (center of mass) of plinabulin within the colchicine site of βII-tubulin (B) and βIII-tubulin (C) computed along our SMD trajectories. Each point represents the spatial localization of the plinabulin's COM according to the following color scheme: red has a probability of >75th percentile, orange has probability within 25th and 75th percentile, and indigo has a probability of <25th percentile.

simulation protocol as described above, running multiple replicas of SMD simulations with the βII-tubulin system in complex with the two compounds, and using the corresponding high-resolution crystal structure as starting points.[40,41] After equilibration, 20 SMD simulations for each system were carried out using a scaling factor of 0.4 and restraining the GTP, the GDP, the Mg^{2+}, and the protein's backbone, with weak positional restraints (harmonic force constant = 50 kJ mol^{-1} nm^{-2}) to prevent unfolding. We excluded from this positional restraint all the residues 6 Å from the inhibitors along with the residues forming the exit channels as identified by the Pocketron analysis[42] (see the Supplemental Information for further details). To compute the residence time of each ligand, we averaged the scaled unbinding time of the 20 SMD simulations and performed a bootstrap analysis. Colchicine showed the highest residence time (97.1 ± 12.9 ns), followed by plinabulin (71.0 ± 10.0 ns, see above), and finally combretastatin-A4 (32.0 ± 4.5 ns), which unbound remarkably faster relative to the two other compounds (Figure 5). These results confirm that the promising molecular properties of plinabulin also from the

Please cite this article in press as: La Sala et al., Structure, Thermodynamics, and Kinetics of Plinabulin Binding to Two Tubulin Isotypes, Chem (2019), https://doi.org/10.1016/j.chempr.2019.08.022

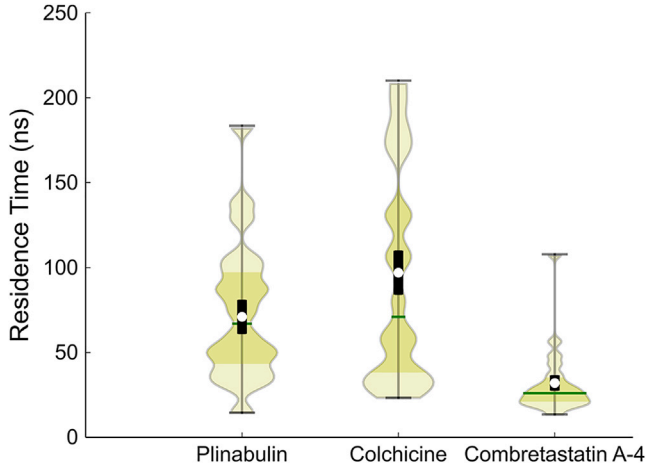

Figure 5. Violin Plots Showing the Distribution of the Residence Time Calculated along the 20 SMD Replicates of the βII-Tubulin-Tail-Plinabulin, βII-Tubulin-Tail-Colchicine, and βII-Tubulin-Tail-Combretastatin-A-4 Systems Using a Kernel Density Estimate

The median (dark green line), the interquartile ranges (dark olive fill), and the 2% and 98% percentiles (black whiskers) are shown. The mean and the standard error computed via bootstrap analysis (white dots and black box, respectively) are also shown. The mean and the standard error computed via bootstrap analysis (white dot and black box, respectively) are also shown. The mean and the standard error of the residence time for plinabulin, colchine, and combretastatin-A4 are 71.0 +/− 10.0 ns, 97.1 +/− 12.9 ns, and 32.0 +/− 4.5 ns, respectively. See also the Supplemental Information.

kinetics standpoint, showing an average residence time between a remarkably slow colchicine-site binder (colchicine[43]) and a rather fast binder (combretastatin-A4[44]). The three ligands utilized the same paths A, B, and C to leave the colchicine site, with a different propensity for one unbinding route over others. Much longer, brute-force MD simulations would provide a more detailed picture of the unbinding mechanisms of plinabulin, colchicine, and combretastatin-A4; however, such simulations are out of the reach of current computational capabilities.

DISCUSSION

The colchicine site is a pocket predominantly located on the β-tubulin subunits of the αβ-tubulin heterodimer, which is targeted by microtubule-destabilizing agents including plinabulin, colchicine, and combretastatin-A4.[16] Human cells express different tubulin isotypes,[45] which results in discrete single amino acid substitutions in the colchicine site. These substitutions likely affect the different selectivity and pharmacological profiles of colchicine-site drugs toward different tubulin isotypes. Indeed, as previously mentioned, the archetypical colchicine-site ligand colchicine displays different binding kinetics and binding affinities toward different β-tubulin isotypes.[6–8] However, a detailed understanding of the differential structural and kinetic properties of colchicine-site binders to different β-tubulin isotypes is largely lacking.

Here, we used X-ray crystallography and MD simulations to study the binding profile of plinabulin toward two different β-tubulin isotypes, βII- and βIII-tubulin. First, we solved the crystal structures of plinabulin bound to both βII- and βIII-tubulin at high resolution. The structures revealed that plinabulin occupies the colchicine site of both tubulin isotypes, displaying a similar binding mode, as the two sites differ by only two residues (βC241 versus βS241 and βI318 versus βV318 in βII-versus βIII-tubulin, respectively). In particular, we noted that the sulfhydryl group of the side

Please cite this article in press as: La Sala et al., Structure, Thermodynamics, and Kinetics of Plinabulin Binding to Two Tubulin Isotypes, Chem (2019), https://doi.org/10.1016/j.chempr.2019.08.022

chain of βC241 of βII-tubulin is located at a greater distance from the carbonyl group of the diketopiperazine ring of plinabulin relative to the hydroxyl group of the side chain of βS241 of βIII-tubulin (i.e., 3.3 Å versus 2.8 Å). Furthermore, the side chain of βC241 existed in two alternate conformations suggesting flexibility. To investigate in depth the free energy difference of ligand binding to the two isotypes, we ran TI starting from both the βII-tubulin-plinabulin and βIII-tubulin-plinabulin systems and performing forward and backward transformations. These calculations revealed a small but consistent difference in terms of binding free energy between the two systems and showed that plinabulin binding is slightly more stable in the colchicine site of βII-tubulin relative to that of βIII-tubulin, possibly due to an entropic gain.

We next studied the binding kinetics with a particular focus on residence time. We calculated the residence time of plinabulin in both the βII- and βIII-tubulin systems. Residence time is a measure of how long a compound stays in contact with its biological target and is emerging as a key parameter for drug discovery and development. It has been argued that the longer the residence time of a drug, the more efficacious the drug will be *in vivo*, and therefore, optimizing this parameter could provide better candidates for subsequent clinical trials.[46,47] We found that plinabulin unbinds slower from the βII- relative to the βIII-tubulin system. The presence of βI318 in βII-tubulin versus βV318 in βIII-tubulin increases the steric hindrance in the colchicine site and could be responsible for the longer residence time observed in βII-tubulin. The residence time is the inverse of the unbinding kinetics constant, k_{off}, and we could therefore conclude that the k_{off} of plinabulin is slower in the βII- than in the βIII-tubulin system. Computational unbinding trajectories also prompted us to investigate the different routes plinabulin departed from the colchicine site to the solvent. In the vast majority of the trajectories, plinabulin leaves the colchicine site through a similar mechanism. A key role was played by the βT7 loop of β-tubulin that can modulate ligand unbinding; it most likely represents the main structural motif in tubulin governing the binding and unbinding kinetics of colchicine-site ligands, in agreement with previous findings.[40] Analyses of all the trajectories have also shown that plinabulin could adopt two possible poses, i.e., the crystallographic pose and a shifted one in which the compound is lodged into an adjacent, small hydrophobic pocket of the colchicine site, which has been recently described by X-ray crystallography.[39] In particular, our analysis indicates that the shifted pose is more likely to exist in βII-tubulin, while in βIII-tubulin, the ligand is confined into the crystallographic pose. This difference in ligand mobility could be responsible for the different entropic gain of plinabulin binding to βII- than βIII-tubulin. Importantly, biochemical assays performed to evaluate the selectivity of plinabulin versus the two tubulin isotypes confirmed our computational and structural outcomes, indicating that the compound displays a higher potency toward the βII- than the βIII-tubulin isoform.

We may speculate that an interesting and perhaps pharmacologically relevant observation is that the nature of the binding of plinabulin within the colchicine site differs from that of colchicine and combretastatin-4A. As shown in Figure 1C, the benzyl and the diketopiperazine-imidazol moieties of plinabulin occupy zones 3 and 2 of the colchicine site, respectively. In contrast, the two archetypical colchicine-site drugs colchicine and combretastatin-A4 occupy zones 1 and 2 in a similar manner and overlap only little with plinabulin (Figure 1D). Notably, the αT5 loop in the tubulin-plinabulin structure is in a "close" conformation, while the ones seen in the tubulin-colchicine and tubulin-combretastatin-A4 structures adopt a more "open" conformation to accommodate the respective ligands in zone 3 of the colchicine site (Figure 1D). These differences might contribute to the unique anti-CIN

Please cite this article in press as: La Sala et al., Structure, Thermodynamics, and Kinetics of Plinabulin Binding to Two Tubulin Isotypes, Chem (2019), https://doi.org/10.1016/j.chempr.2019.08.022

effect of plinabulin (not demonstrated by either of the other MTAs), the good cardiac safety profile, and the activation of the immune-oncology system by plinabulin. These observations may lay the basis for subsequent investigations aimed at providing further clues about the relationships between the tubulin inhibition mechanism of plinabulin and its unique therapeutic profile.

Based on the present studies, we propose that plinabulin is more persistently bound to the colchicine site of βII-tubulin relative to that of βIII-tubulin. This conclusion is supported by the following three main observations: (1) in βII-tubulin, plinabulin is lodged into a wider pocket with a possible entropic gain able to compensate for the higher force of the observed hydrogen bond with βS241 in βIII-tubulin versus βC241 in βII-tubulin; (2) the plinabulin residence time is longer in βII- than βIII-tubulin, showing that binding is more persistent within the βII-tubulin system, most likely because of the presence of βI318 in βII-tubulin versus βV318 in βIII-tubulin; and (3) plinabulin is more active toward βII- relative to βIII-tubulin in biochemical experiments. Overall, these observations may support the idea that plinabulin displays a higher potency toward βII-tubulin overexpressing cancer cells than those overexpressing βIII-tubulin. Clearly, systematic cellular analyses with cancer cells overexpressing one of the two isotypes will be necessary to validate our predictions.

Next, we compared the residence time of plinabulin with that of two anti-tubulin compounds, colchicine and combretastatin-A4, using an SMD protocol and the high-resolution crystallographic structures of these molecules in complex with tubulin. SMD-based residence time of plinabulin (~71 ns) is longer than that of the very fast scaled residence time of combretastatin-A4 (~32 ns) and more similar to but slower than that of the long unbinding time of colchicine (~97 ns; note that colchicine binding occurs in two steps, a fast binding step and a slow conformational change that locks the ligand into the binding site[48]). In patients, colchicine is associated with diarrhea, nausea, cramping, abdominal pain, and vomiting,[49] while combretastatin-A4 is associated with cardiovascular side effects[17] significantly beyond the transient (on the order of hours) hypertensive effects reported with plinabulin.[16,50] It is notable that the most common side effects of plinabulin in cancer patients are associated with the gastrointestinal system,[16,50] although far less severe than observed with colchicine. Our data therefore indicate a possible correlation of toxicity profile and residence time in colchicine binding, with long residence time associated with gastrointestinal toxicity and short residence time associated with cardiotoxicity. In this sense, plinabulin may approach an ideal balance allowing for establishing efficacy with an acceptable toxicity by achieving a residence time and gastrointestinal-cardiac toxicity profile midway between colchicine and combretastatin-A4. This may be further supported by reports that both colchicine[18] and combretastatin-A4[19] cause an adverse reduction in the number of circulating neutrophils (neutropenia), while plinabulin actually prevents neutropenia induced by chemotherapy.[51] These hypotheses will certainly need further experimental validations to gather a superior understanding of the complex mechanism(s) underlying associations between tubulin-binding versus effect profile.

EXPERIMENTAL PROCEDURES

Crystallization and X-Ray Data Collection

The recombinant tubulin was expressed and purified as previously described.[27] The bovine brain tubulin was purchased from the Centro de Investigaciones Biológicas (CSIC, Madrid, Spain). Proteins and crystals of the TD1 complex (a protein complex containing one tubulin dimer and the tubulin-binding darpin D1[52]) were prepared as

Please cite this article in press as: La Sala et al., Structure, Thermodynamics, and Kinetics of Plinabulin Binding to Two Tubulin Isotypes, Chem (2019), https://doi.org/10.1016/j.chempr.2019.08.022

described previously.[53] Briefly, co-crystallization experiments were performed in parallel for bovine brain and recombinant tubulin by diluting a freshly prepared 50 mM plinabulin stock solution (in 100% DMSO) to 5 mM with the crystallization solution (100 mM Bis-TrisMethane, pH 5.5, supplemented with 200 mM ammonium sulfate and 25% PEG3350). 1 μL of $T_{\beta II}D1$ or $T_{\beta III}D1$ at 15 mg/mL was mixed with 1 μL of the 5 mM plinabulin and equilibrated against 400 μL of the crystallization solution using the hanging drop vapor diffusion method. Crystals appeared overnight, were flash-frozen in liquid nitrogen, and were used directly for X-ray diffraction experiments at 100K at the X06DA beamline of the Swiss Light Source (Paul Scherrer Institut, Villigen, Switzerland) using a standard protocol.

Structure Solution

Data processing was performed using the XDS software package.[54] Both the $T_{\beta II}D1$-plinabulin and $T_{\beta III}D1$-plinabulin complexes crystallized in the space group $P12_11$ with a single molecule in the asymmetric unit. Structure solution was performed by the molecular replacement method using a previously published TD1 structure (i.e., containing αIβII-tubulin as tubulin model; PDB ID 4DRX) after removing all the ligands and solvent molecules, by using the program PHASER in the PHENIX software package.[55] Similar to $T_{\beta II}D1$-plinabulin, the $T_{\beta III}D1$-plinabulin structure was solved by molecular replacement using the $T_{\beta II}D1$-plinabulin structure without the ligand as a model. Plinabulin was added to the model using eLBOW in PHENIX, and its structure was further refined through iterative rounds of model building in Coot[56] and PHENIX. The quality of the structure was assessed with MolProbity[57] Data collection and refinement statistics are presented in Table S1. Figures were prepared using PyMOL (The PyMOL Molecular Graphics System, Version 2.2.3. Schrödinger).

Structural Models for Computational Studies

In this work, we employed two molecular systems, namely βII-tubulin-plinabulin and βIII-tubulin-plinabulin. The two complexes were prepared, starting from the solved $T_{\beta II}D1$-plinabulin and $T_{\beta III}D1$-plinabulin X-ray crystal structures after the removal of the tubulin-binding darpin D1. Missing residues and loops were built using the PDB ID 5LYJ as template.[40] The co-crystalized GTP, GDP, Mg^{2+}, and plinabulin were retained as well as the water molecules in the plinabulin-binding site. To parameterize the GTP and GDP cofactors, we employed the available parameters from the Amber database.[58] BiKi Life Sciences suite[59] was employed to parameterize plinabulin. Charges were computed at HF/6-31G* level of theory and fitted via the RESP procedure,[60] while the General Amber Force Field (Gaff)[61] was employed to parameterize the bonded and vdW terms of plinabulin. Tubulin, instead, was parameterized using Amber14SB force field.[62] These two final structures were employed for both TI and MM/GBSA calculations.

In the case of SMD simulations, the C-terminal tails were included in both the α- and β-tubulin subunits, and these two systems are referred to as βII-tubulin-tail-plinabulin and βIII-tubulin-tail-plinabulin. Since the predicted unbinding times might be affected by the electrostatic environment of the systems, we decided to include the highly negatively charged C-terminal tails in order not to neglect their possible influence in the plinabulin residence time. The preparation of these two systems, as well as the preparation of the βII-tubulin-colchicine and βII-tubulin-combretastatin A-4 systems, are reported in the Supplemental Information.

MM/GBSA Calculations

We performed MM/GBSA calculations to compare the binding free energy (i.e., $\Delta G_{bind(MMPBSA)}$) between plinabulin and the βII- and βIII-tubulin systems. The final

Please cite this article in press as: La Sala et al., Structure, Thermodynamics, and Kinetics of Plinabulin Binding to Two Tubulin Isotypes, Chem (2019), https://doi.org/10.1016/j.chempr.2019.08.022

$\Delta G_{bind(MMPBSA)}$ estimation is averaged using a trajectory of classical MD simulations of both βII-tubulin-plinabulin and βIII-tubulin-plinabulin systems. The two parameterized systems (see the previous section) were solvated using TIP3P[63] waters and neutralized adding Na^+ counterions using the tleap module in AmberTools17. The equilibration of both βII-tubulin-plinabulin and βIII-tubulin-plinabulin systems consisted of six steps: (1) minimization of water molecules combining steepest descent and conjugate gradient methods, restraining the complex; (2) 20 ps at 300 K to relax the water molecules, while the complex is still restrained; (3) minimization of whole system combining steepest descent and conjugate gradient methods; (4) heating of the system in 500 ps in NVT ensemble, reaching a target temperature of 300 K using Berendsen thermostat,[64] restraining the complex; (5) adjusting the density of the system in 500 ps in NPT ensemble. A target temperature of 1 bar was reached using Berendsen barostat, while temperature was regulated using Langevin dynamics and a collision frequency γ of 2 ps^{-1}. Also in this case, the complex was maintained restrained; (6) final 5 ns in NPT using the same settings as in (5) and releasing the restraints. After the equilibration, 100 ns of plain MD simulations in NPT ensemble were run for each of the two systems. The simulations were run by means of pmemd engine, implemented in Amber 16. For MM/GBSA estimation, we extracted one frame every 400 ps from the original trajectory, for a total of 250 frames. To run MM/GBSA analysis, we employed the MMPBSA.py Python script present in Amber16, employing the mbondi2 radii and using a modified GB model developed by Onufriev et al.[65]

Free Energy Differences via Thermodynamic Integration Calculations

In this study, we performed thermodynamic integration (TI) calculations to estimate the relative binding free energy difference between plinabulin and the βII-tubulin-plinabulin and βIII-tubulin-plinabulin systems, see Structural Models for Computational Studies). To do so, we took advantage of multi-step alchemical transformations to gradually transform the plinabulin-binding site from βII- to βIII-tubulin and vice versa, upon the mutation of two side chains: the βC241 and βI318 that are transformed into βS241 and βV318, respectively, in the case of βII → βIII transformation; and βS241 and βV318 that are transformed into βC241 and βI318 in the case of βIII → βII transformation. The free energy loss or gain associated to these transformations are computed via the TI formalism[66] (see below).

We performed a total of 8 alchemical transformations, as reported in Table 1 and Figure 2. Four transformations have as starting point the βII-tubulin-plinabulin system. Here, the βII-tubulin-binding site is gradually transformed into βIII-tubulin by first mutating βC241 to a serine (βII/TR_1) and then mutating βI318 to valine (βII/TR_2). Also, the backward transformations are performed (βII/TR_3 and βII/TR_4). The remaining four transformations, instead, have as starting point the βIII– and βIII-tubulin-plinabulin systems. Here, the βIII-tubulin-binding site is gradually transformed into βII-tubulin by first replacing βS241 to a cysteine (βIII/TR_1) and then mutating βV318 to an isoleucine (βIII/TR_2). Also in this case, the backward transformations are carried out (βIII/TR_3 and βIII/TR_4). For each of the 8 transformations, we employed the same simulations protocol that is detailed in the Supplemental Information.

Scaled MD Simulations

The solvated βII-tubulin-tail-plinabulin and βIII-tubulin-tail-plinabulin systems (see the Supplemental Information) were first equilibrated using the same protocol employed for the modeling of the tubulin with the C-terminal tails (see the Supplemental Information). Then, 20 SMD simulations for each system were carried out

Please cite this article in press as: La Sala et al., Structure, Thermodynamics, and Kinetics of Plinabulin Binding to Two Tubulin Isotypes, Chem (2019), https://doi.org/10.1016/j.chempr.2019.08.022

using a scaling factor of 0.4 and restraining the GTP, the GDP, the Mg^{2+} and the protein's backbone, with weak positional restraints whose harmonic force constant was set 50 kJ mol^{-1} nm^{-2} to prevent the unfolding of the protein. We excluded from this selection all the residues 6 Å from plinabulin along with residues forming the unbinding channel, which connects the binding pocket to the bulk of the solvent (see the Supplemental Information). We computed the residence time of plinabulin and the associated standard error (SE) in both the βII- and βIII-tubulin systems, averaging the residence time of the 20 SMD simulations and performing a bootstrap analysis as reported in the study of Mollica et al.[33] The same procedure was then utilized for colchicine and combretastatin-A4 for making a comparison, in terms of residence time, among different colchicine-site inhibitors (see the Supplemental Information for further details).

Differential Effect of Plinabulin on βII- and βIII-tubulin

Samples containing 60 μM bovine brain tubulin (58% βII, 25% βIII, and 17% other tubulin isotypes; [30]) were incubated in GAB buffer (3.4 M glycerol, 10 mM sodium phosphate, 1 mM EGTA, 1 mM GTP, pH 6.7) at 37 C for 1 h in the absence or presence of 5 μM plinabulin. The samples were then centrifuged for 20 min at 5,000 rpm in a Beckman Optima TLX in 200 μL polycarbonate tubes. Supernatants were collected, and pellets were resuspended in GAB buffer. The amount of protein in the supernatants and pellets were quantified by the bicinchoninic acid (BCA) assay[67] in order to load equal amounts of tubulin in each well. For western blots, 1 or 0.2 μg of tubulin was load per well of a 15% SDS-PA Gel. Samples (3×) were subject to SDS-PAGE and transferred to a nitrocellulose membrane using the Trans-Blot® Turbo Blotting System (Bio-rad) for 10 min. The membranes were blocked by incubation with 6% milk in phosphate-buffered saline (PBS) 0.1 % Tween 20 at room temperature for 1 h. Then they were incubated with the primary antibodies anti-βII (Sigma-Aldrich, 1/200) and anti-βIII (Sigma-Aldrich, 1/1,500) at 4°C overnight. Membranes were washed three times with PBST for 10 min and incubated with the secondary antibody (donkey a-mouse, 1/10,000) for 1 h at room temperature. Finally, the membranes were washed three times with PBST for 10 min and exposed with the ECL reagent. Images were taken using a ChemiDocTM instrument (Bio-rad) and analyzed with the Image Lab 5.2.1 software (Bio-rad).

SUPPLEMENTAL INFORMATION

Supplemental Information can be found online at https://doi.org/10.1016/j.chempr.2019.08.022.

ACKNOWLEDGMENTS

We thank Shih-Chieh Ti and Tarun Kapoor for providing human recombinant tubulin samples. X-ray diffraction data were collected at the beamline X06DA at the Swiss Light Source (Paul Scherrer Institut, Villigen PSI, Switzerland). We thank Dr. Dario Gioia for useful discussions. This work was financially supported by BeyondSpring Pharmaceuticals (to M.O.S. and A.C.) and by grants from the Ministerio de Ciencia, Innovación y Universidades (BFU2016-75319-R to J.F.D.), the Swiss National Science Foundation (31003A_166608 to M.O.S.) and the Regione Lombardia (Accordo per la Ricerca e l'Innovazione).

AUTHOR CONTRIBUTIONS

L.H., J.R.T., G.K.L., J.F.D., M.O.S., and A.C. designed the research. G.L.S., N.O., A.S., F.V., F.D. A.B.P., and S.D. performed experiments. All the authors analyzed the data and wrote the paper.

Please cite this article in press as: La Sala et al., Structure, Thermodynamics, and Kinetics of Plinabulin Binding to Two Tubulin Isotypes, Chem (2019), https://doi.org/10.1016/j.chempr.2019.08.022

DECLARATION OF INTERESTS

The authors declare the following financial interests: L.H., J.K.L., and J.R.T. are employed by BeyondSpring Pharmaceuticals and have an equity (stock) interest in the company.

Received: March 17, 2019
Revised: July 2, 2019
Accepted: August 23, 2019
Published: September 23, 2019

REFERENCES

1. Dumontet, C., and Jordan, M.A. (2010). Microtubule-binding agents: a dynamic field of cancer therapeutics. Nat. Rev. Drug Discov. *9*, 790–803.

2. Steinmetz, M.O., and Prota, A.E. (2018). Microtubule-targeting agents: strategies to hijack the cytoskeleton. Trends Cell Biol. *28*, 776–792.

3. Li, W., Sun, H., Xu, S., Zhu, Z., and Xu, J. (2017). Tubulin inhibitors targeting the colchicine binding site: a perspective of privileged structures. Future Med. Chem. *9*, 1765–1794.

4. Kavallaris, M. (2010). Microtubules and resistance to tubulin-binding agents. Nat. Rev. Cancer *10*, 194–204.

5. Tame, M.A., Manjón, A.G., Belokhvostova, D., Raaijmakers, J.A., and Medema, R.H. (2017). TUBB3 overexpression has a negligible effect on the sensitivity to taxol in cultured cell lines. Oncotarget *8*, 71536–71547.

6. Banerjee, A., and Luduena, R.F. (1992). Kinetics of colchicine binding to purified beta-tubulin isotypes from bovine brain. J. Biol. Chem. *267*, 13335–13339.

7. Borisy, G.G., and Taylor, E.W. (1967). The mechanism of action of colchicine. Binding of colchincine-3H to cellular protein. J. Cell Biol. *34*, 525–533.

8. Borisy, G.G., and Taylor, E.W. (1967). The mechanism of action of colchicine. Colchicine binding to sea urchin eggs and the mitotic apparatus. J. Cell Biol. *34*, 535–548.

9. Minoura, I., Hachikubo, Y., Yamakita, Y., Takazaki, H., Ayukawa, R., Uchimura, S., and Muto, E. (2013). Overexpression, purification, and functional analysis of recombinant human tubulin dimer. FEBS Lett. *587*, 3450–3455.

10. Nicholson, B., Lloyd, G.K., Miller, B.R., Palladino, M.A., Kiso, Y., Hayashi, Y., and Neuteboom, S.T.C. (2006). NPI-2358 is a tubulin-depolymerizing agent: in-vitro evidence for activity as a tumor vascular-disrupting agent. Anticancer Drugs *17*, 25–31.

11. Yamazaki, Y., Kohno, K., Yasui, H., Kiso, Y., Akamatsu, M., Nicholson, B., Deyanat-Yazdi, G., Neuteboom, S., Potts, B., Lloyd, G.K., et al. (2008). Tubulin photoaffinity labeling with biotin-tagged derivatives of potent diketopiperazine antimicrotubule agents. Chembiochem *9*, 3074–3081.

12. Wang, Y., Zhang, H., Gigant, B., Yu, Y., Wu, Y., Chen, X., Lai, Q., Yang, Z., Chen, Q., and Yang, J. (2016). Structures of a diverse set of colchicine binding site inhibitors in complex with tubulin provide a rationale for drug discovery. FEBS J. *283*, 102–111.

13. Yamazaki, Y., Sumikura, M., Masuda, Y., Hayashi, Y., Yasui, H., Kiso, Y., Chinen, T., Usui, T., Yakushiji, F., Potts, B., et al. (2012). Synthesis and structure–activity relationships of benzophenone-bearing diketopiperazine-type anti-microtubule agents. Bioorg. Med. Chem. *20*, 4279–4289.

14. Yamazaki, Y., Tanaka, K., Nicholson, B., Deyanat-Yazdi, G., Potts, B., Yoshida, T., Oda, A., Kitagawa, T., Orikasa, S., Kiso, Y., et al. (2012). Synthesis and structure–activity relationship study of antimicrotubule agents phenylahistin derivatives with a Didehydropiperazine-2,5-dione structure. J. Med. Chem. *55*, 1056–1071.

15. Hayashi, Y., Yamazaki-Nakamura, Y., and Yakushiji, F. (2013). Medicinal chemistry and chemical biology of diketopiperazine-type antimicrotubule and vascular-disrupting agents. Chem. Pharm. Bull. (Tokyo) *61*, 889–901.

16. Mita, M.M., Spear, M.A., Yee, L.K., Mita, A.C., Heath, E.I., Papadopoulos, K.P., Federico, K.C., Reich, S.D., Romero, O., Malburg, L., et al. (2010). Phase 1 first-in-human trial of the vascular disrupting agent plinabulin(NPI-2358) in patients with solid tumors or lymphomas. Clin. Cancer Res. *16*, 5892–5899.

17. Subbiah, I.M., Lenihan, D.J., and Tsimberidou, A.M. (2011). Cardiovascular toxicity profiles of vascular-disrupting agents. Oncologist *16*, 1120–1130.

18. Harris, R., Marx, G., Gillett, M., Kark, A., and Arunanthy, S. (2000). Colchicine-induced bone marrow suppression: treatment with granulocyte colony-stimulating factor. J. Emerg. Med. *18*, 435–440.

19. Grisham, R., Ky, B., Tewari, K.S., Chaplin, D.J., and Walker, J. (2018). Clinical trial experience with CA4P anticancer therapy: focus on efficacy, cardiovascular adverse events, and hypertension management. Gynecol. Oncol. Res. Pract. *5*, 1.

20. NCT02504489-Assessment of Docetaxel + Plinabulin Compared to Docetaxel + Placebo in Patients with Advanced NSCLC with at Least One Measurable Lung Lesion (DUBLIN-3). (2015). https://clinicaltrials.gov/ct2/show/NCT02504489.

21. NCT03102606-Plinabulin vs. Pegfilgrastim in Patients with Solid Tumors Receiving Docetaxel Myelosuppressive Chemotherapy. (2017). https://clinicaltrials.gov/ct2/show/NCT03102606.

22. Tozer, G.M., Kanthou, C., Parkins, C.S., and Hill, S.A. (2002). The biology of the combretastatins as tumour vascular targeting agents. Int. J. Exp. Pathol. *83*, 21–38.

23. Tron, G.C., Pirali, T., Sorba, G., Pagliai, F., Busacca, S., and Genazzani, A.A. (2006). Medicinal chemistry of combretastatin A4: present and future directions. J. Med. Chem. *49*, 3033–3044.

24. Prota, A.E., Bargsten, K., Zurwerra, D., Field, J.J., Díaz, J.F., Altmann, K.H., and Steinmetz, M.O. (2013). Molecular mechanism of action of microtubule-stabilizing anticancer agents. Science *339*, 587–590.

25. Ravelli, R.B.G., Gigant, B., Curmi, P.A., Jourdain, I., Lachkar, S., Sobel, A., and Knossow, M. (2004). Insight into tubulin regulation from a complex with colchicine and a stathmin-like domain. Nature *428*, 198–202.

26. Massarotti, A., Coluccia, A., Silvestri, R., Sorba, G., and Brancale, A. (2012). The tubulin colchicine domain: a molecular modeling perspective. ChemMedChem *7*, 33–42.

27. Ti, S.C., Pamula, M.C., Howes, S.C., Duellberg, C., Cade, N.I., Kleiner, R.E., Forth, S., Surrey, T., Nogales, E., and Kapoor, T.M. (2016). Mutations in human tubulin proximal to the kinesin-binding site alter dynamic instability at microtubule plus- and Minus-ends. Dev. Cell *37*, 72–84.

28. Genheden, S., and Ryde, U. (2015). The MM/PBSA and MM/GBSA methods to estimate ligand-binding affinities. Expert Opin. Drug Discov. *10*, 449–461.

29. Hou, T., Wang, J., Li, Y., and Wang, W. (2011). Assessing the performance of the MM/PBSA and MM/GBSA methods. 1. The accuracy of binding free energy calculations based on molecular dynamics simulations. J. Chem. Inf. Model. *51*, 69–82.

30. Banerjee, A., Roach, M.C., Trcka, P., and Luduena, R.F. (1992). Preparation of a monoclonal antibody specific for the class IV isotype of beta-tubulin. Purification and assembly of alpha beta II, alpha beta III, and alpha beta IV tubulin dimers from bovine brain. J. Biol. Chem. *267*, 5625–5630.

31. Sáez-Calvo, G., Sharma, A., Balaguer, F.A., Barasoain, I., Rodríguez-Salarichs, J., Olieric, N., Muñoz-Hernández, H., Berbís, M.Á., Wendeborn, S., Peñalva, M.A., et al. (2017). Triazolopyrimidines are microtubule-stabilizing agents that bind the vinca inhibitor site of tubulin. Cell Chem. Biol. *24*, 737–750.e6.

32. Banerjee, A., Roach, M.C., Trcka, P., and Ludueña, R.F. (1990). Increased microtubule assembly in bovine brain tubulin lacking the type III isotype of beta-tubulin. J. Biol. Chem. *265*, 1794–1799.

33. Mollica, L., Decherchi, S., Zia, S.R., Gaspari, R., Cavalli, A., and Rocchia, W. (2015). Kinetics of protein-ligand unbinding via smoothed potential molecular dynamics simulations. Sci. Rep. *5*, 11539.

34. Mollica, L., Theret, I., Antoine, M., Perron-Sierra, F., Charton, Y., Fourquez, J.M., Wierzbicki, M., Boutin, J.A., Ferry, G., Decherchi, S., et al. (2016). Molecular Dynamics simulations and kinetic measurements to estimate and predict protein–ligand residence times. J. Med. Chem. *59*, 7167–7176.

35. Schuetz, D.A., Bernetti, M., Bertazzo, M., Musil, D., Eggenweiler, H.M., Recanatini, M., Masetti, M., Ecker, G.F., and Cavalli, A. (2019). Predicting residence time and drug unbinding pathway through scaled Molecular Dynamics. J. Chem. Inf. Model. *59*, 535–549.

36. Bernetti, M., Rosini, E., Mollica, L., Masetti, M., Pollegioni, L., Recanatini, M., and Cavalli, A. (2018). Binding residence time through scaled molecular dynamics: a prospective application to hDAAO inhibitors. J. Chem. Inf. Model. *58*, 2255–2265.

37. Bernetti, M., Masetti, M., Rocchia, W., and Cavalli, A. (2019). Kinetics of drug binding and residence time. Annu. Rev. Phys. Chem. *70*, 143–171.

38. Yamazaki, Y., Sumikura, M., Hidaka, K., Yasui, H., Kiso, Y., Yakushiji, F., and Hayashi, Y. (2010). Anti-microtubule 'plinabulin' chemical probe KPU-244-B3 labeled both α- and β-tubulin. Bioorg. Med. Chem. *18*, 3169–3174.

39. Fu, Z., Hou, Y., Ji, C., Ma, M., Tian, Z., Deng, M., Zhong, L., Chu, Y., and Li, W. (2018). Design, synthesis and biological evaluation of anti-pancreatic cancer activity of plinabulin derivatives based on the co-crystal structure. Bioorg. Med. Chem. *26*, 2061–2072.

40. Gaspari, R., Prota, A.E., Bargsten, K., Cavalli, A., and Steinmetz, M.O. (2017). Structural Basis of cis- and trans -combretastatin binding to tubulin. Chem *2*, 102–113.

41. Prota, A.E., Danel, F., Bachmann, F., Bargsten, K., Buey, R.M., Pohlmann, J., Reinelt, S., Lane, H., and Steinmetz, M.O. (2014). The novel microtubule-destabilizing drug BAL27862 binds to the colchicine site of tubulin with distinct effects on microtubule organization. J. Mol. Biol. *426*, 1848–1860.

42. La Sala, G., Decherchi, S., De Vivo, M., and Rocchia, W. (2017). Allosteric communication networks in proteins revealed through pocket crosstalk analysis. ACS Cent. Sci. *3*, 949–960.

43. Fernando Díaz, J.F., and Andreu, J.M. (1991). Kinetics of dissociation of the tubulin-colchicine complex. Complete reaction scheme and comparison to thermodynamic measurements. J. Biol. Chem. *266*, 2890–2896.

44. Lin, C.M., Ho, H.H., Pettit, G.R., and Hamel, E. (1989). Antimitotic natural products combretastatin A-4 and combretastatin A-2: studies on the mechanism of their inhibition of the binding of colchicine to tubulin. Biochemistry *28*, 6984–6991.

45. Nogales, E. (2000). Structural insights into microtubule function. Annu. Rev. Biochem. *69*, 277–302.

46. Copeland, R.A., Pompliano, D.L., and Meek, T.D. (2006). Drug-target residence time and its implications for lead optimization. Nat. Rev. Drug Discov. *5*, 730–739.

47. Copeland, R.A. (2016). The drug-target residence time model: a 10-year retrospective. Nat. Rev. Drug Discov. *15*, 87–95.

48. Lambeir, A., and Engelborghs, Y. (1981). A fluorescence stopped flow study of colchicine binding to tubulin. J. Biol. Chem. *256*, 3279–3282.

49. Hood, R.L. (1994). Colchicine poisoning. J. Emerg. Med. *12*, 171–177.

50. Millward, M., Mainwaring, P., Mita, A., Federico, K., Lloyd, G.K., Reddinger, N., Nawrocki, S., Mita, M., and Spear, M.A. (2012). Phase 1 study of the novel vascular disrupting agent plinabulin (NPI-2358) and docetaxel. Investig. New Drugs *30*, 1065–1073.

51. Blayney, D.W., Bazhenova, L., Lloyd, G.K., Huang, L., and Mohanlal, R. (2016). Plinabulin, a novel small molecule that ameliorates chemotherapy-induced neutropenia, is administered on the same day of chemotherapy and has anticancer efficacy. Blood *128*, 2508.

52. Pecqueur, L., Duellberg, C., Dreier, B., Jiang, Q., Wang, C., Plückthun, A., Surrey, T., Gigant, B., and Knossow, M. (2012). A designed ankyrin repeat protein selected to bind to tubulin caps the microtubule plus end. Proc. Natl. Acad. Sci. USA *109*, 12011–12016.

53. Sharma, A., Aher, A., Dynes, N.J., Frey, D., Katrukha, E.A., Jaussi, R., Grigoriev, I., Croisier, M., Kammerer, R.A., Akhmanova, A., et al. (2016). Centriolar CPAP/SAS-4 imparts slow processive microtubule growth. Dev. Cell *37*, 362–376.

54. Kabsch, W. (2010). XDS. Acta Crystallogr. D Biol. Crystallogr. *66*, 125–132.

55. Adams, P.D., Afonine, P.V., Bunkóczi, G., Chen, V.B., Davis, I.W., Echols, N., Headd, J.J., Hung, L.W., Kapral, G.J., Grosse-Kunstleve, R.W., et al. (2010). *PHENIX*: a comprehensive Python-based system for macromolecular structure solution. Acta Crystallogr. D Biol. Crystallogr. *66*, 213–221.

56. Emsley, P., Lohkamp, B., Scott, W.G., and Cowtan, K. (2010). Features and development of *coot*. Acta Crystallogr. D Biol. Crystallogr. *66*, 486–501.

57. Chen, V.B., Arendall, W.B., Headd, J.J., Keedy, D.A., Immormino, R.M., Kapral, G.J., Murray, L.W., Richardson, J.S., and Richardson, D.C. (2010). *MolProbity*: all-atom structure validation for macromolecular crystallography. Acta Crystallogr. D Biol. Crystallogr. *66*, 12–21.

58. Meagher, K.L., Redman, L.T., and Carlson, H.A. (2003). Development of polyphosphate parameters for use with the AMBER force field. J. Comput. Chem. *24*, 1016–1025.

59. Decherchi, S., Bottegoni, G., Spitaleri, A., Rocchia, W., and Cavalli, A. (2018). BiKi Life Sciences: a new suite for molecular dynamics and related methods in drug discovery. J. Chem. Inf. Model. *58*, 219–224.

60. Cornell, W.D., Cieplak, P., Bayly, C.I., and Kollman, P.A. (1993). Application of RESP charges to calculate conformational energies, hydrogen bond energies, and free energies of solvation. J. Am. Chem. Soc. *115*, 9620–9631.

61. Wang, J., Wolf, R.M., Caldwell, J.W., Kollman, P.A., and Case, D.A. (2004). Development and testing of a general amber force field. J. Comput. Chem. *25*, 1157–1174.

62. Maier, J.A., Martinez, C., Kasavajhala, K., Wickstrom, L., Hauser, K.E., and Simmerling, C. (2015). ff14SB: improving the accuracy of protein side chain and backbone parameters from ff99SB. J. Chem. Theor. Comput. *11*, 3696–3713.

63. Jorgensen, W.L., Chandrasekhar, J., Madura, J.D., Impey, R.W., and Klein, M.L. (1983). Comparison of simple potential functions for simulating liquid water. J. Chem. Phys. *79*, 926–935.

64. Berendsen, H.J.C., Postma, J.P.M., van Gunsteren, W.F., DiNola, A., and Haak, J.R. (1984). Molecular Dynamics with coupling to an external bath. J. Chem. Phys. *81*, 3684–3690.

65. Onufriev, A., Bashford, D., and Case, D.A. (2004). Exploring protein native states and large-scale conformational changes with a modified generalized born model. Proteins *55*, 383–394.

66. Kollman, P. (1993). Free energy calculations: applications to chemical and biochemical phenomena. Chem. Rev. *93*, 2395–2417.

67. Smith, P.K., Krohn, R.I., Hermanson, G.T., Mallia, A.K., Gartner, F.H., Provenzano, M.D., Fujimoto, E.K., Goeke, N.M., Olson, B.J., and Klenk, D.C. (1985). Measurement of protein using bicinchoninic acid. Anal. Biochem. *150*, 76–85.

Chem, Volume *5*

Supplemental Information

Structure, Thermodynamics, and Kinetics of Plinabulin Binding to Two Tubulin Isotypes

Giuseppina La Sala, Natacha Olieric, Ashwani Sharma, Federica Viti, Francisco de Asis Balaguer Perez, Lan Huang, James R. Tonra, G. Kenneth Lloyd, Sergio Decherchi, José Fernando Díaz, Michel O. Steinmetz, and Andrea Cavalli

Supplemental Experimental Procedures

Modeling of tubulin with C-terminal tails. To account for a possible influence of the negatively charged, disordered C-terminal tail regions of α- and β-tubulin on the residence time of the ligands, we modeled these elements to obtain the two new biomolecular systems namely βII-tubulin-tail-plinabulin and βIII-tubulin-tail-plinabulin. Starting from βII-tubulin-plinabulin and βIII-tubulin-plinabulin systems, we manually added the missing residues of the α– and β–subunits letting them to adopt a starting 3D extended conformation. Using the BiKi Life Sciences suite[1], we solvated the systems using TIP3P[2] water molecules, leaving a buffer of 12 Å between the solute and the box edges. Each solvated system was then neutralized by replacing water molecules with an appropriated number of Na^+ counter ions. The final complexes were minimized and equilibrated to reach a target temperature of 300 K and a final pressure of 1 bar. Three simulations of 500 ps each were run in the NVT ensemble, using the velocity rescaling thermostat to gradually heat the system to 100, 200 and 300 K. The protein backbone and the ligands heavy atoms (i.e., plinabulin, GTP, GDP and Mg^{2+}) were restrained using a harmonic restraint with force constant of 1000 kJ mol^{-1} nm^{-2}. The last equilibration step of 500 ps was run in the NPT ensemble to adjust the density of the system, using the velocity rescaling thermostat[3] and the Parrinello-Rahman barostat,[4] (releasing the restraints). Finally, ~140 ns of SMD simulations using a scaling factor of 0.8 were carried out to enhance the exploration of the conformational space of the two C-terminal tails. To avoid the unfolding of the protein, weak positional restraints (harmonic force constant = 50 kJ mol^{-1} nm^{-2}) were applied to the ligands and to the backbone of the protein, with the exception of the two C-terminal tails. The P-LINCS algorithm[5] was employed to restraint bonds involving hydrogen atoms in their equilibrium length. Long-range electrostatics were treated with the Particle mesh Ewald (PME) method,[6] while periodic boundary conditions were applied in the three dimensions. Both system equilibration and SMD simulations were performed using the BiKi Life Sciences suite. In order to retrieve the most probable final conformations of both the α– and β subunit C-terminal tails, we run a cluster analysis on the SMD trajectory, were we extracted the medoids of the most populated clusters. These two medoids were used as starting points for the next SMD simulations.

Models of βII-tubulin in complex with colchicine and combretastatin A-4. Besides plinabulin, we also investigated the kinetic profiles of the two tubulin inhibitors colchicine and combretastatin A-4 in complex with βII-tubulin. These two systems are referred to as βII-tubulin-colchicine and βII-tubulin-combretastatinA-4. The two systems were prepared starting from the PDB codes 4O2B and 5LYJ, removing the other crystallographic protein units (i.e., stathmin-like protein RB3 and tubulin tyrosine ligase). The missing residues present in the X-ray structures were filled using the "fix structure" tool implemented in the BiKi suite. The missing C-terminal tails were built using as template the βII-tubulin-tail-plinabulin system. Also in this case, the protein in both the βII-tubulin-colchicine and II-tubulin-combretastatinA-4 systems was parameterized with the Amber ff14SB force field[7], whereas the GTP and GDP parameters were retrieved from the Bryce database (http://research.bmh.manchester.ac.uk/bryce/amber).[8] The charges of colchicine were computed using BiKi at HF/6-31G* level of theory and fitted via the RESP procedure[9], while the General Amber Force Field (Gaff)[10] was employed to parameterize the bonded terms. The combretastatin A-4 parameters were

the ones used in Gaspari et al.[11] For both systems, we employed the same procedure mentioned above for solvating and neutralizing the systems.

Selection of restraints in SMD simulations. In order to define the unrestrained residues for SMD simulations, we performed a preliminary analysis to identify a possible channel within the tubulin dimer that might favor unbinding of the ligands (i.e., plinabulin, colchicine and combretastatin A-4). In particular, we performed a ~90 ns long SMD using the βII-tubulin-tail-plinabulin system applying a scaling factor of 0.45 and applying weak positional restraints (harmonic restraints force constant = 50 kJ mol-1 nm-2) to the GTP, GDP and the protein's backbone with the exception of the residues 6 Å away from plinabulin. Then, we run the Pocketron tool[12] implemented in the BiKi 1.3 suite,[1] to identify and track all the pockets formed along SMD simulations. We used a radius 3 and 1.5 Å for the big and the small probe, respectively, and discarded from the analysis all the pockets that are smaller than the volume occupied by 3 water molecules. Using this approach, we were able to identify putative channels that might help the departure of the ligands from the colchicine site and that are not detectable by only the visual inspection of crystallographic structures. Therefore, we added to the previously mentioned unrestrained residues also the residues that formed these new channels. The unrestrained residues were: αQ176, αV177, αS178, αT179, αA180, αT223, αY224, αT225, αI455, βF20, βV51, βY52, βQ136, βI165, βN167, βF169, βE200, βY208, βV238, βT239, βT240, βS241, βL242, βR243, βF244, βP245, βG246, βQ247, βL248, βN249, βA250, βD251, βL252, βL255, βM259, βV315, βA316, βT317, βV318, βF319, βR320, βG321, βR322, βM323, βS324, βM325, βP348, βN349, βN350, βV351, βK352, βV353, βA354, βV355, βC356, βD357, βT376, βI378 (βIII-tubulin X-ray numbering, see Figure S3). For consistency, we adopted the same set of unrestrained residues for all SMD simulations.

Thermodynamic integration protocols. For each of the 8 transformations (i.e. βII/*TR*$_1$, βII/*TR*$_2$, βII/*TR*$_3$, βII/*TR*$_4$, βIII/*TR*$_1$, βIII/*TR*$_2$, βIII/*TR*$_3$ and βIII/*TR*$_4$) we employed the same simulative protocol. The starting system was firstly equilibrated at λ = 0.5. The equilibration consisted of a minimization, a 20 ps long thermalization at 300 K using the Berendsen thermostat and a 40 ps short equilibration to adjust the density of the system using again the Berendsen barostat.[13] The coordinates of the equilibrated system at λ = 0.5 were used as starting point for the simulations for the other λ values. For each transformation, we run 11 simulations for the tubulin-plinabulin complex and 11 simulations for the protein alone (see Figure 2). We used a window size of Δλ = 0.1, where the starting system is λ = 0.0 and the final system is λ = 1.0. For each λ value, 200 ps of constant volume equilibration was followed by 10 ns of constant pressure production. The starting systems for the first two transformations (i.e., βII/TR$_1$ and βIII/TR$_1$) are βII-tubulin-plinabulin and βIII-tubulin-plinabulin (see above), while the intermediate starting systems for other transformations were modeled by manually mutating the residue of interest.

For each transformation, the free energy (ΔG) associated to move from the initial to the final one is:

$$\Delta G = \int_0^1 \langle \frac{\delta U}{\delta \lambda} \rangle \, d\lambda \qquad (1)$$

where U is the potential energy of the system and λ is the parameter that varies the potential from the initial state (λ=0.0) to the final state (λ=1.0). Therefore, according to the alchemical cycle depicted in Figure 2, the binding free energy difference of plinabulin from protein A to protein B is: $\Delta\Delta G_{bind[A \to B]} = \Delta G_{bound[A \to B]}$ -

$\Delta G_{unbound[A \rightarrow B]}$, where the first term corresponds to the free energy gained/lost computed with formula (1) to transform the protein from the initial (A) to the final state (B) when in complex with the ligand, whereas the second term is analogous but the ligand is not bound to the protein. The convergence of TI simulations was assessed by estimating the $\Delta\Delta G_{bind}$ as a function of the simulation time,[8] interrupting the MD simulations when the $\Delta\Delta G_{bind}$ values reached the plateau as depicted in Figure S4. All the simulations were performed using a single-step approach, where electrostatic and the van der Waals softcore potential terms are switched at the same time for each λ value Simulations were performed using the pmemd module implemented in Amber16.[15]

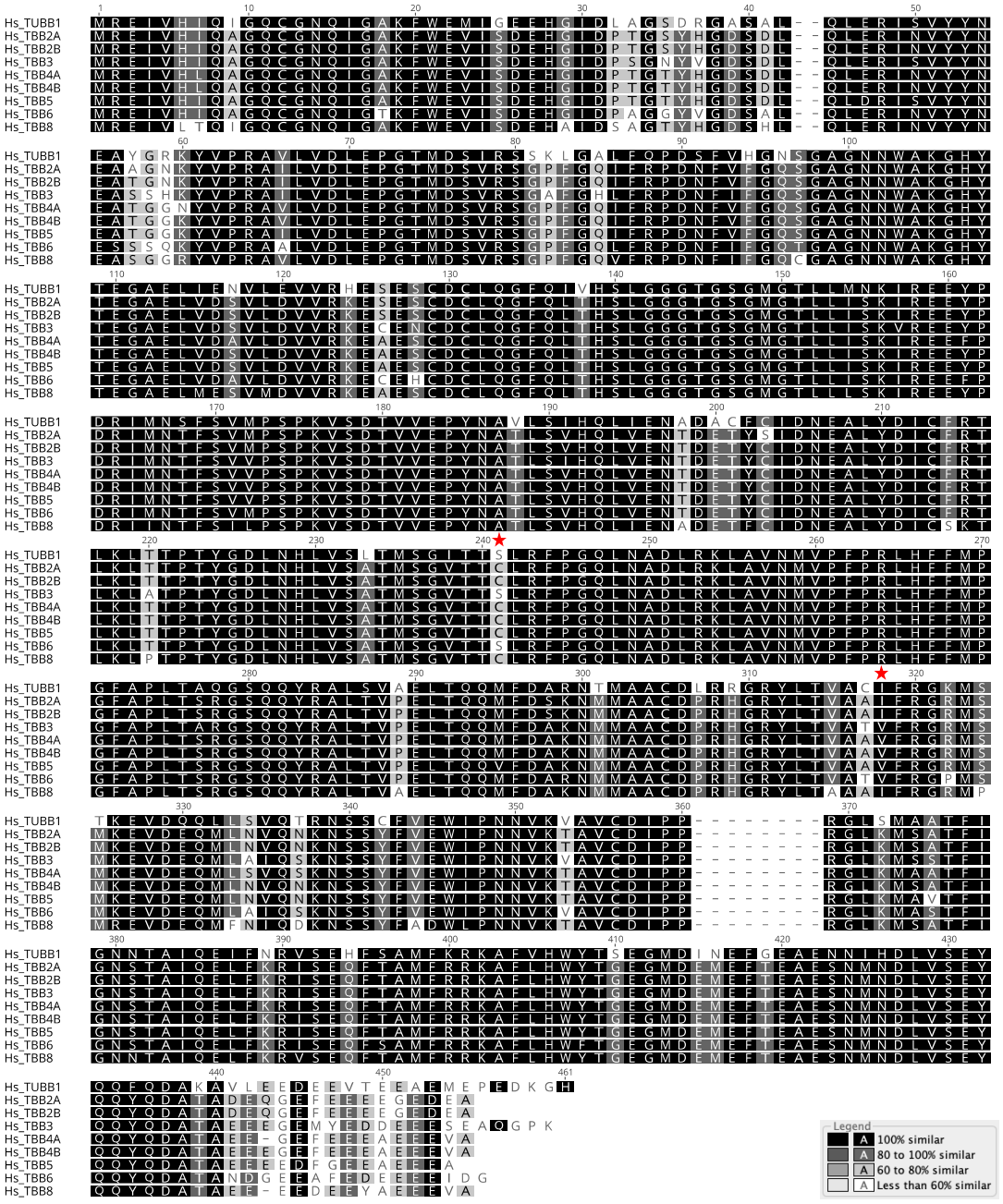

Figure S1. Alignment of human β -tubulin isotypes (uniprot codes of the sequences from top to bottom in the alignment: Q9H4B7, Q13885, Q9BVA1, Q13509, P04350, P68371, P07437, Q9BUF5, Q3ZCM7) using Geneious Prime (Biomatters Ltd.). Red stars on top of the alignment highlights amino acid differences involved in plinabulin binding. Gaps were introduced manually to match residues numbering with alpha tubulin as defined by Lowe et al.[16]

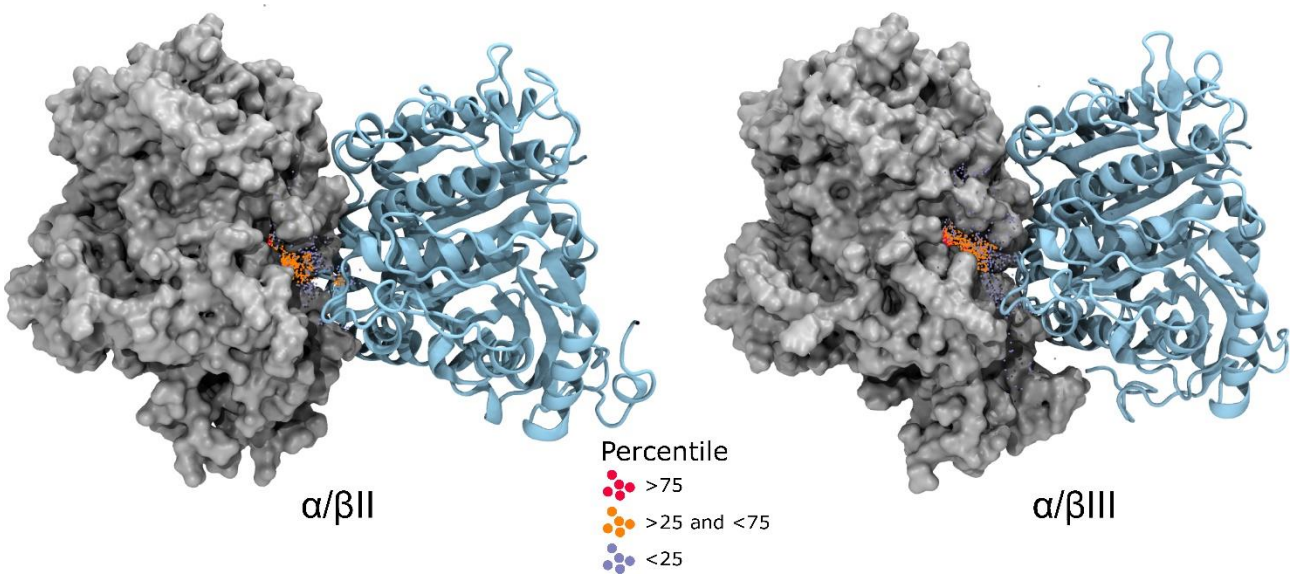

Figure S2. Representation of the probability of finding the COM (center of mass) of plinabulin for the βII- (left side) and tubulin (right side) systems computed along the SMD trajectories. Each point represents the spatial localization of plinabulin's COM according to the following color scheme: red has a probability of >75 percentile, orange has a probability within 25 and 75 percentile, and indigo has probability <25 percentile.

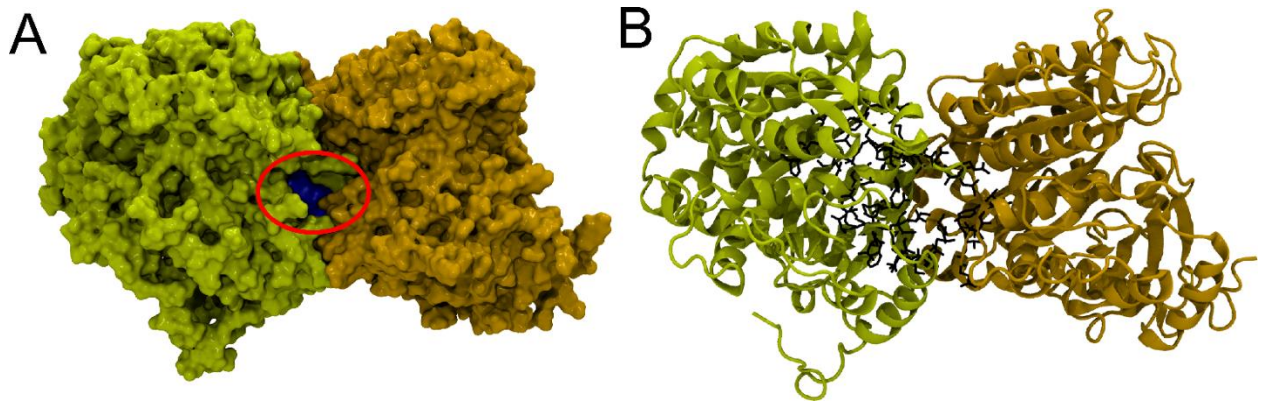

Figure S3. A) Representation of the α (orange) and β (yellow) chains of the βII-tubulin system. The blue pocket circled in red represents the possible departure channel of the binders of the colchicine site. The structure belongs to a representative frame extracted from SMD simulations. B) In black sticks the residues of both the colchicine site and the departure channel that are not restrained in the SMD trajectories of the βII-tubulin-tail-plinabulin, βIII-tubulin-tail-plinabulin, βII-tubulin-tail-colchicine and βII-tubulin-tail-combretastatinA-4 systems are represented.

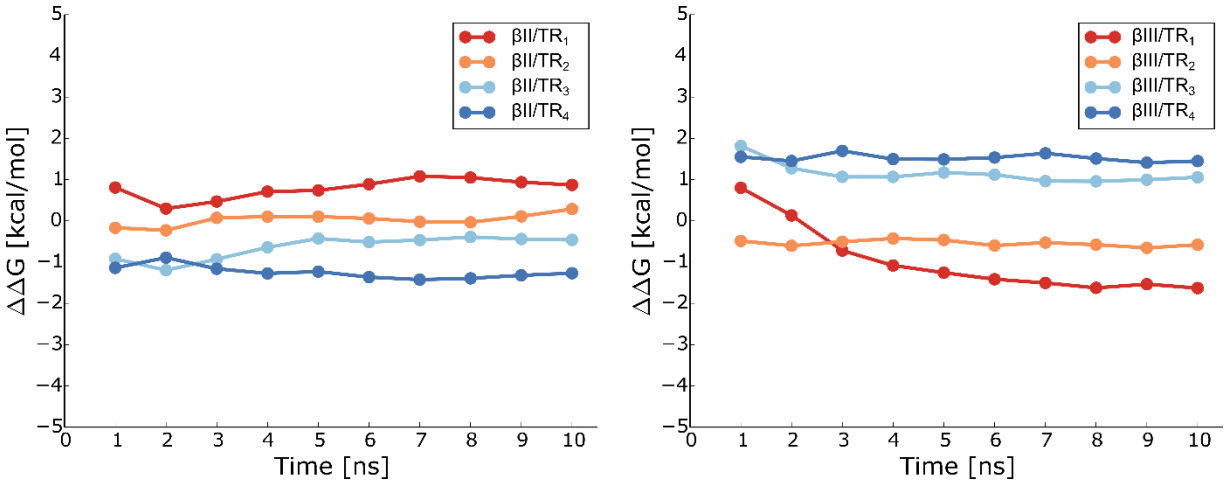

Figure S4. Free energy convergence in time for both the four transformations related to βII→βIII($βII_{mut-2}$) in the left panel and the four transformations related to βIII→βII($βIII_{mut-2}$) in the right panel.

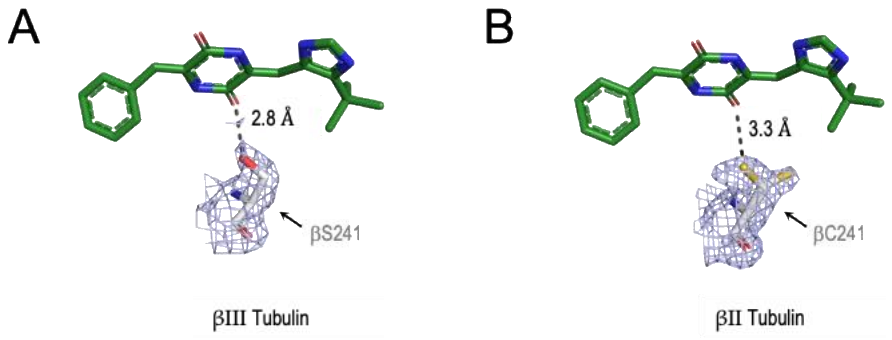

Figure S5. Electron density showing the conformation of the S241 side chain in the $T_{βIII}$D1-plinabulin structure (A) and the C241 side chain in the $T_{βII}$D1-plinabulin structure (B). Plinabulin is shown in green sticks representation. Electron densities are displayed using a sigma A weighted 2Fo-Fc map contoured at 1.0 level using Pymol.

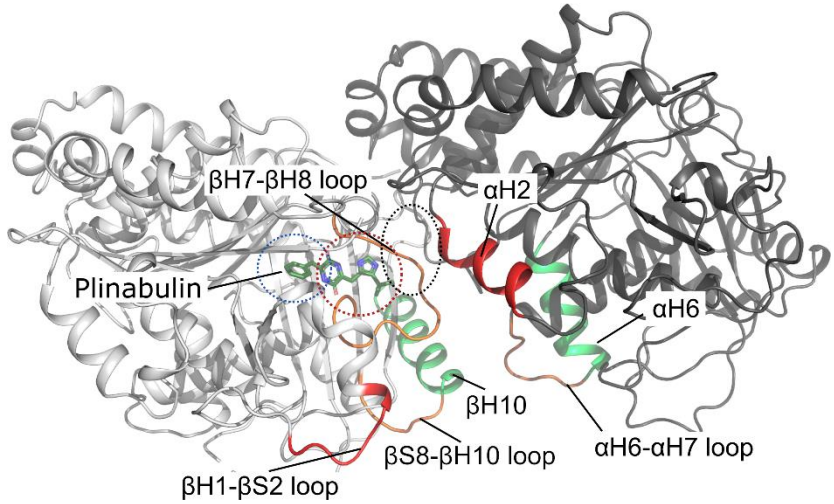

Figure S6. Representation of the three exit pathways evidenced in our SMD simulations. The alpha and the beta tubulin are represented in grey and white cartoon, respectively. We oriented the dimer in the same way as in Figure 1 of the main text and adopted the same colors for the exit pathways as in Figure 3 of the main text. The colored circles in the Plinabulin binding site represent zone 1,2 and 3 (black, red and blue, respectively). The orange, red and green portions of the protein represent, instead, the path A, B and C.

Data Collection[a]	$T_{\beta II}$D1-Plinabulin	$T_{\beta III}$D1-Plinabulin
Wavelength, Å	1	1
Space group	P 1 21 1	P 1 21 1
Resolution range, Å	45.02 – 1.519 (1.574 - 1.519)	45.6 – 1.801 (1.865 – 1.801)
Unit cell a, b, c (Å) , , (°)	73.565 91.351 83.221 90 96.851 90	73.63 91.2 82.64 90 97.493 90
No. of observed reflections	1127765 (103861)	651489 (60526)
No. of unique reflections	166365 (15828)	98394 (5181)
Mean I/sigma(I)	16.43 (1.21)	11.04 (1.29)
R-merge	0.05515 (1.52)	0.1429 (1.894)
R-meas	0.05971 (1.648)	0.1555 (2.071)
CC1/2[b]	0.999 (0.683)	0.996 (0.419)
CC*	1 (0.901)	0.999 (0.768)
Refinement		
R-work	0.1764 (0.3644)	0.2256 (0.3567)
R-free	0.2023 (0.3726)	0.2622 (0.3658)
Macromolecules	8072	7817
Ligands	86	87
Protein residues	1017	999
RMS (bonds) (Å)	0.008	0.011
RMS (angles) (°)	1.13	1.26
Ramachandran favored (%)[c]	98.61	98.27
Ramachandran outliers (%)[c]	0	0
B-factors		
Average B-factor	37.17	25.51
Macromolecules	36.35	25.01
Ligands	27.68	17.21
Solvent	45.45s	31.45

[a] Highest resolution shell statistics are in parentheses.
[b] As defined by Karplus and Diederichs.[17]
[c] As defined by MolProbity.[18]

Table S1. X-Ray data collection and refinement statistics.

Supplemental References

1. Decherchi, S., Bottegoni, G., Spitaleri, A., Rocchia, W., and Cavalli, A. (2018). BiKi Life Sciences: A New Suite for Molecular Dynamics and Related Methods in Drug Discovery. J. Chem. Inf. Model. *58*, 219–224.

2. Jorgensen, W.L., Chandrasekhar, J., Madura, J.D., Impey, R.W., and Klein, M.L. (1983). Comparison of simple potential functions for simulating liquid water. J. Chem. Phys. *79*, 926–935.

3. Bussi, G., Donadio, D., and Parrinello, M. (2007). Canonical sampling through velocity rescaling. J. Chem. Phys. *126*, 014101.

4. Parrinello, M., and Rahman, A. (1981). Polymorphic transitions in single crystals: A new molecular dynamics method. J. Appl. Phys. *52*, 7182–7190.

5. Hess, B. (2008). P-LINCS: A Parallel Linear Constraint Solver for Molecular Simulation. J. Chem. Theory Comput. *4*, 116–122.

6. Essmann, U., Perera, L., Berkowitz, M.L., Darden, T., Lee, H., and Pedersen, L.G. (1995). A smooth particle mesh Ewald method. J. Chem. Phys. *103*, 8577–8593.

7. Maier, J.A., Martinez, C., Kasavajhala, K., Wickstrom, L., Hauser, K.E., and Simmerling, C. (2015). ff14SB: Improving the Accuracy of Protein Side Chain and Backbone Parameters from ff99SB. J. Chem. Theory Comput. *11*, 3696–3713.

8. Meagher, K.L., Redman, L.T., and Carlson, H.A. (2003). Development of polyphosphate parameters for use with the AMBER force field. J. Comput. Chem. *24*, 1016–1025.

9. Cornell, W.D., Cieplak, P., Bayly, C.I., and Kollman, P.A. (1993). Application of RESP charges to calculate conformational energies, hydrogen bond energies, and free energies of solvation. J. Am. Chem. Soc. *115*, 9620–9631.

10. Wang, J., Wolf, R.M., Caldwell, J.W., Kollman, P.A., and Case, D.A. (2004). Development and testing of a general amber force field. J. Comput. Chem. *25*, 1157–1174.

11. Gaspari, R., Prota, A.E., Bargsten, K., Cavalli, A., and Steinmetz, M.O. (2017). Structural Basis of cis - and trans -Combretastatin Binding to Tubulin. Chem *2*, 102–113.

12. La Sala, G., Decherchi, S., De Vivo, M., and Rocchia, W. (2017). Allosteric Communication Networks in Proteins Revealed through Pocket Crosstalk Analysis. ACS Cent. Sci. *3*, 949–960.

13. Berendsen, H.J.C., Postma, J.P.M., van Gunsteren, W.F., DiNola, A., and Haak, J.R. (1984). Molecular dynamics with coupling to an external bath. J. Chem. Phys. *81*, 3684–3690.

14. Klimovich, P.V., Shirts, M.R., and Mobley, D.L. (2015). Guidelines for the analysis of free energy calculations. J. Comput. Aided Mol. Des. *29*, 397–411.

15. Kaus, J.W., Pierce, L.T., Walker, R.C., and McCammon, J.A. (2013). Improving the Efficiency of Free Energy Calculations in the Amber Molecular Dynamics Package. J. Chem. Theory Comput. *9*, 4131–4139.

16. Löwe, J., Li, H., Downing, K.H., and Nogales, E. (2001). Refined structure of alpha beta-tubulin at 3.5 A resolution. J. Mol. Biol. *313*, 1045–1057.

17. Karplus, P. A. and Diederichs, K. (2012). Linking crystallographic model and data quality. Science 336, 1030-1033.

18. Davis, I.W., Murray, L. W., Richardson, J. S. and Richardson, D. C. (2004). MOLPROBITY: structure validation and all-atom contact analysis for nucleic acids and their complexes. Nucleic Acids Res. 32, W615-W619.